

Two-Higgs-doublet models in light of current experiments: a brief review

Lei Wang¹, Jin Min Yang^{2,3}, Yang Zhang⁴

¹ *Department of Physics, Yantai University, Yantai 264005, P. R. China*

² *CAS Key Laboratory of Theoretical Physics, Institute of Theoretical Physics, Chinese Academy of Sciences, Beijing 100190, P. R. China*

³ *School of Physical Science, University of Chinese Academy of Sciences, Beijing 100049, P. R. China*

⁴ *School of Physics and Microelectronics, Zhengzhou University, Zhengzhou 450001, P. R. China*

ABSTRACT: We briefly survey several typical CP-conserving two-Higgs-doublet models (2HDMs) in light of current experiments. First we derive the masses and couplings of the mass eigenstates from the Lagrangians. Then we analyze the constraints from theory and oblique electroweak parameters. Finally, we delineate the status of 2HDM in light of the LHC searches, the dark matter detections and the muon $g - 2$ measurement.

Contents

1	Introduction	2
2	Several typical 2HDMs	3
2.1	Type-I, type-II, lepton-specific and flipped 2HDMs	3
2.2	Inert Higgs doublet model	6
3	Constraints from theory and oblique parameters	6
3.1	Vacuum stability	6
3.2	Unitarity	7
3.3	Oblique parameters	9
4	Constraints from LHC searches for Higgs bosons	12
4.1	Signal data of the 125 GeV Higgs	12
4.2	Searches for additional scalars at LHC	14
5	Dark matter observables	17
5.1	Inert 2HDM and dark matter	17
5.2	Wrong-sign Yukawa couplings and isospin-violating interactions between dark matter and nucleons.	17
6	Muon anomalous magnetic moment	19
6.1	L2HDM and muon $g - 2$	19
6.2	Solution of muon $g - 2$ and τ decays	24
6.2.1	Lepton specific inert 2HDM	25
6.2.2	μ - τ -philic Higgs doublet model	27
6.3	Other 2HDMs and muon $g - 2$	29
7	Summary	29
	Acknowledgments	30

1 Introduction

A two-Higgs-doublet model (2HDM) is a simple extension of the Standard Model (SM) by introducing an additional $SU(2)_L$ Higgs doublet, which predicts three neutral Higgs bosons and a pair of charged Higgs bosons H^\pm . The 2HDM can be CP-violating [1], but it is also useful to study its CP conserving version, where the neutral Higgs bosons can be classified into the CP-even states (h and H) and the CP-odd state (A). The tree-level flavour changing neutral current (FCNC) can appear in the general 2HDM, which is forbidden by imposing Z_2 discrete symmetry in several different ways, such as type-I 2HDM [2, 3], type-II 2HDM [2, 4], lepton-specific 2HDM (L2HDM), flipped 2HDM [5–10], and inert 2HDM [11–13]. Also the tree-level FCNC is absent in the aligned 2HDM in which the Yukawa-coupling matrices of the two Higgs doublet fields are assumed to be proportional [14]. In addition, due to certain type of symmetry, the FCNC is naturally suppressed by the off-diagonal element of the CKM matrix in the Branco-Grimus-Lavoura (BGL) 2HDM [15].

Various 2HDMs have been extensively studied in particle physics. Because of the plenty Yukawa couplings of the quarks and leptons, the 2HDMs have been studied in meson decays, and the L2HDM is used to explain the muon $g - 2$ anomaly [16–33]. In the inert 2HDM, one may take the lightest component of the inert Higgs doublet field is neutral, and consider it as a dark matter (DM) candidate because of its stability. If an additional field protected by a new symmetry is added to other types of 2HDMs, then these models also can provide a DM candidate. In these models, the multiple scalar fields can be as the portals between the DM and the SM sector, and lead to some interesting effects on the DM observables via their various Yukawa couplings [34–50]. On the other hand, the analyses of ATLAS and CMS collaborations at the LHC show that the properties of the discovered 125 GeV Higgs boson agree well with the SM Higgs boson [51, 52]. Other than that, no experiment claims to have observed any new resonance with 5σ level. However, there are some interesting excesses which imply the existence of new scalars. For example, the CMS Run II results for Higgs boson searches in the diphoton final state show a local excess of $\sim 3\sigma$ around 96 GeV [53]. The ATLAS collaboration reported a local excess of $\sim 3\sigma$ around 130 GeV in the searches for $t \rightarrow H^\pm b$ with $H^\pm \rightarrow cb$ [54]. Besides, very recently the CDF II result for the W -mass has an approximate 7σ discrepancy from the SM prediction [55]. The 2HDM can give additional corrections to the masses of gauge bosons via the self-energy diagrams exchanging extra Higgs fields, and simply explain the CDF W -mass when the extra Higgses have appropriate mass splittings (see e.g., [56–69]).

In the literature there already have been some reviews on 2HDMs (see e.g., [70–75]). In this note we emphasize current experiments and briefly review several typical CP-conserving 2HDMs. We will start from the Lagrangians and derive the masses and couplings of the particles. Then we analyze the constraints from theory and oblique electroweak parameters, respectively. Finally, we discuss the status of 2HDMs in light of the LHC searches, the dark matter detections and the muon $g - 2$ measurement.

The content is organized as follows. In Sections II and III, we demonstrate several typical

CP-conserving 2HDMs and discuss the constraints from theory and oblique parameters. In Sections IV, V, and VI, we review the status of the 2HDMs in light of the LHC Higgs searches, the DM detections and the muon $g - 2$ measurement. Finally, we give a summary in Section 7.

2 Several typical 2HDMs

The general scalar potential of 2HDM is given as

$$\begin{aligned}
V_{\text{tree}} = & m_{11}^2(\Phi_1^\dagger\Phi_1) + m_{22}^2(\Phi_2^\dagger\Phi_2) - m_{12}^2(\Phi_1^\dagger\Phi_2 + \text{h.c.}) \\
& + \frac{\lambda_1}{2}(\Phi_1^\dagger\Phi_1)^2 + \frac{\lambda_2}{2}(\Phi_2^\dagger\Phi_2)^2 + \lambda_3(\Phi_1^\dagger\Phi_1)(\Phi_2^\dagger\Phi_2) + \lambda_4(\Phi_1^\dagger\Phi_2)(\Phi_2^\dagger\Phi_1) \\
& + \left[\frac{\lambda_5}{2}(\Phi_1^\dagger\Phi_2)^2 + \lambda_6(\Phi_1^\dagger\Phi_1)(\Phi_1^\dagger\Phi_2) + \lambda_7(\Phi_2^\dagger\Phi_2)(\Phi_1^\dagger\Phi_2) + \text{h.c.} \right], \quad (2.1)
\end{aligned}$$

and the Φ_1 and Φ_2 are complex Higgs doublets with hypercharge $Y = 1$:

$$\Phi_1 = \begin{pmatrix} \phi_1^+ \\ \frac{1}{\sqrt{2}}(v_1 + \phi_1 + ia_1) \end{pmatrix}, \quad \Phi_2 = \begin{pmatrix} \phi_2^+ \\ \frac{1}{\sqrt{2}}(v_2 + \phi_2 + ia_2) \end{pmatrix}. \quad (2.2)$$

Here we restrict to the CP-conserving models in which all λ_i and m_{12}^2 are real and the electroweak vacuum expectation values (VEVs) v_1 and v_2 are also real with $v^2 = v_1^2 + v_2^2 = (246 \text{ GeV})^2$.

2.1 Type-I, type-II, lepton-specific and flipped 2HDMs

In order to forbid tree-level FCNC, one may introduce an additional Z_2 discrete symmetry under which the charge assignments of fields are shown in Table 1. Because of this Z_2 symmetry, the λ_6 and λ_7 terms in the general scalar potential in Eq. (2.1) are absent, while the soft breaking m_{12}^2 term is still allowed. The mass parameters m_{11}^2 and m_{22}^2 in the potential are determined by the potential minimization conditions at (v_1, v_2) :

$$\begin{aligned}
m_{11}^2 = & m_{12}^2 t_\beta - \frac{1}{2} v^2 (\lambda_1 c_\beta^2 + \lambda_{345} s_\beta^2), \\
m_{22}^2 = & m_{12}^2 / t_\beta - \frac{1}{2} v^2 (\lambda_2 s_\beta^2 + \lambda_{345} c_\beta^2), \quad (2.3)
\end{aligned}$$

where the shorthand notations $t_\beta \equiv \tan \beta = v_2/v_1$, $s_\beta \equiv \sin \beta$, $c_\beta \equiv \cos \beta$, and $\lambda_{345} = \lambda_3 + \lambda_4 + \lambda_5$ are employed.

Table 1. The Z_2 charge assignment in the four types of 2HDMs without FCNC. The other fields are even under Z_2 symmetry.

Model	Φ_2	Φ_1	u_R^i	d_R^i	e_R^i
Type I	+	-	+	+	+
Type II	+	-	+	-	-
Lepton-specific	+	-	+	+	-
Flipped	+	-	+	-	+

From the scalar potential in Eq. (2.1) with $\lambda_6 = \lambda_7 = 0$, we can obtain the mass matrices of the Higgs fields

$$\begin{pmatrix} \phi_1 & \phi_2 \end{pmatrix} \begin{pmatrix} m_{12}^2 t_\beta + \lambda_1 v^2 c_\beta^2 & -m_{12}^2 + \frac{\lambda_{345}}{2} v^2 s_{2\beta} \\ -m_{12}^2 + \frac{\lambda_{345}}{2} v^2 s_{2\beta} & m_{12}^2 / t_\beta + \lambda_2 v^2 s_\beta^2 \end{pmatrix} \begin{pmatrix} \phi_1 \\ \phi_2 \end{pmatrix}, \quad (2.4)$$

$$\begin{pmatrix} a_1 & a_2 \end{pmatrix} \left[m_{12}^2 - \frac{1}{2} \lambda_5 v^2 s_{2\beta} \right] \begin{pmatrix} t_\beta & -1 \\ -1 & 1/t_\beta \end{pmatrix} \begin{pmatrix} a_1 \\ a_2 \end{pmatrix}, \quad (2.5)$$

$$\begin{pmatrix} \phi_1^+ & \phi_2^+ \end{pmatrix} \left[m_{12}^2 - \frac{1}{4} (\lambda_4 + \lambda_5) v^2 s_{2\beta} \right] \begin{pmatrix} t_\beta & -1 \\ -1 & 1/t_\beta \end{pmatrix} \begin{pmatrix} \phi_1^- \\ \phi_2^- \end{pmatrix}. \quad (2.6)$$

The mass eigenstates are obtained from the original fields by the rotation matrices:

$$\begin{pmatrix} H \\ h \end{pmatrix} = \begin{pmatrix} \cos \alpha & \sin \alpha \\ -\sin \alpha & \cos \alpha \end{pmatrix} \begin{pmatrix} \phi_1 \\ \phi_2 \end{pmatrix}, \quad (2.7)$$

$$\begin{pmatrix} G^0 \\ A \end{pmatrix} = \begin{pmatrix} \cos \beta & \sin \beta \\ -\sin \beta & \cos \beta \end{pmatrix} \begin{pmatrix} a_1 \\ a_2 \end{pmatrix}, \quad (2.8)$$

$$\begin{pmatrix} G^\pm \\ H^\pm \end{pmatrix} = \begin{pmatrix} \cos \beta & \sin \beta \\ -\sin \beta & \cos \beta \end{pmatrix} \begin{pmatrix} \phi_1^\pm \\ \phi_2^\pm \end{pmatrix}, \quad (2.9)$$

where G^0 and G^\pm are Goldstone bosons which are absorbed as longitudinal components of the Z and W^\pm bosons. The remained physical states are two neutral CP-even states h and H , one neutral pseudoscalar A , and a pair of charged scalars H^\pm . Their masses are given by

$$m_{H,h}^2 = \frac{1}{2} \left[M_{P,11}^2 + M_{P,22}^2 \pm \sqrt{(M_{P,11}^2 - M_{P,22}^2)^2 + 4(M_{P,12}^2)^2} \right], \quad (2.10)$$

$$m_A^2 = \frac{m_{12}^2}{s_\beta c_\beta} - \lambda_5 v^2, \quad (2.11)$$

$$m_{H^\pm}^2 = \frac{m_{12}^2}{s_\beta c_\beta} - \frac{1}{2} (\lambda_4 + \lambda_5) v^2, \quad (2.12)$$

where M_P^2 is the mass matrix shown in Eq. 2.4.

Table 2. The κ_u , κ_d , and κ_ℓ for the four types of 2HDMs.

	type-I	type-II	lepton-specific	flipped
κ_u	$1/t_\beta$	$1/t_\beta$	$1/t_\beta$	$1/t_\beta$
κ_d	$1/t_\beta$	$-t_\beta$	$1/t_\beta$	$-t_\beta$
κ_ℓ	$1/t_\beta$	$-t_\beta$	$-t_\beta$	$1/t_\beta$

The gauge-kinetic Lagrangian is given as

$$\mathcal{L}_g = (D^\mu \Phi_1)^\dagger (D_\mu \Phi_1) + (D^\mu \Phi_2)^\dagger (D_\mu \Phi_2). \quad (2.13)$$

We can obtain the neutral Higgs couplings to VV ($VV \equiv ZZ, WW$)

$$\begin{aligned} \mathcal{L}_g \supset & \frac{g^2 + g'^2}{8} v^2 ZZ \left(1 + 2\frac{h}{v} y_h^V + 2\frac{H}{v} y_H^V \right) \\ & + \frac{g^2}{4} v^2 W^+ W^- \left(1 + 2\frac{h}{v} y_h^V + 2\frac{H}{v} y_H^V \right), \end{aligned} \quad (2.14)$$

where $y_h^V = \sin(\beta - \alpha)$ and $y_H^V = \cos(\beta - \alpha)$.

According to different charge assignments, there are four different models with Yukawa interactions:

$$-\mathcal{L} = Y_{u2} \bar{Q}_L \tilde{\Phi}_2 u_R + Y_{d2} \bar{Q}_L \Phi_2 d_R + Y_{\ell 2} \bar{L}_L \Phi_2 e_R + \text{h.c.} \quad (\text{type I}), \quad (2.15)$$

$$-\mathcal{L} = Y_{u2} \bar{Q}_L \tilde{\Phi}_2 u_R + Y_{d1} \bar{Q}_L \Phi_1 d_R + Y_{\ell 1} \bar{L}_L \Phi_1 e_R + \text{h.c.} \quad (\text{type II}), \quad (2.16)$$

$$-\mathcal{L} = Y_{u2} \bar{Q}_L \tilde{\Phi}_2 u_R + Y_{d1} \bar{Q}_L \Phi_2 d_R + Y_{\ell 1} \bar{L}_L \Phi_1 e_R + \text{h.c.} \quad (\text{lepton specific}), \quad (2.17)$$

$$-\mathcal{L} = Y_{u2} \bar{Q}_L \tilde{\Phi}_2 u_R + Y_{d1} \bar{Q}_L \Phi_1 d_R + Y_{\ell 1} \bar{L}_L \Phi_2 e_R + \text{h.c.} \quad (\text{flipped model}), \quad (2.18)$$

where $Q_L^T = (u_L, d_L)$, $L_L^T = (\nu_L, l_L)$, $\tilde{\Phi}_{1,2} = i\tau_2 \Phi_{1,2}^*$, and Y_{u2} , $Y_{d1,2}$ and $Y_{\ell 1,2}$ are 3×3 matrices in family space.

We can obtain the Yukawa couplings

$$\begin{aligned} -\mathcal{L}_Y = & \frac{m_f}{v} y_h^f h \bar{f} f + \frac{m_f}{v} y_H^f H \bar{f} f \\ & -i \frac{m_u}{v} \kappa_u A \bar{u} \gamma_5 u + i \frac{m_d}{v} \kappa_d A \bar{d} \gamma_5 d + i \frac{m_\ell}{v} \kappa_\ell A \bar{\ell} \gamma_5 \ell \\ & + H^+ \bar{u} V_{\text{CKM}} \left(\frac{\sqrt{2} m_d}{v} \kappa_d P_R - \frac{\sqrt{2} m_u}{v} \kappa_u P_L \right) d + \text{h.c.} \\ & + \frac{\sqrt{2} m_\ell}{v} \kappa_\ell H^+ \bar{\nu} P_R e + \text{h.c.} \end{aligned} \quad (2.19)$$

where $y_h^f = \sin(\beta - \alpha) + \cos(\beta - \alpha) \kappa_f$ and $y_H^f = \cos(\beta - \alpha) - \sin(\beta - \alpha) \kappa_f$. The values of κ_u , κ_d and κ_ℓ for the four models are shown in Table 2.

2.2 Inert Higgs doublet model

We impose an exact Z_2 discrete symmetry in the 2HDM and assume that it remains after the potential minimization. Under the Z_2 symmetry all the SM fields are taken to be even, while the new (inert) doublet Φ_2 is odd:

$$\Phi_1 = \begin{pmatrix} G^+ \\ \frac{1}{\sqrt{2}}(v + h + iG) \end{pmatrix}, \quad \Phi_2 = \begin{pmatrix} H^+ \\ \frac{1}{\sqrt{2}}(H + iA) \end{pmatrix}. \quad (2.20)$$

The Φ_1 field has a vev $v = 246$ GeV, and Φ_2 has no vev.

The scalar potential is

$$\begin{aligned} \mathcal{V} = & m_{11}^2(\Phi_1^\dagger\Phi_1) + m_{22}^2(\Phi_2^\dagger\Phi_2) + \frac{\lambda_1}{2}(\Phi_1^\dagger\Phi_1)^2 + \frac{\lambda_2}{2}(\Phi_2^\dagger\Phi_2)^2 \\ & + \lambda_3(\Phi_1^\dagger\Phi_1)(\Phi_2^\dagger\Phi_2) + \lambda_4(\Phi_1^\dagger\Phi_2)(\Phi_2^\dagger\Phi_1) + \left[\frac{\lambda_5}{2}(\Phi_1^\dagger\Phi_2)^2 + \text{h.c.} \right]. \end{aligned} \quad (2.21)$$

The parameter m_{11}^2 is fixed by the scalar potential minimum conditions

$$m_{11}^2 = -\frac{1}{2}\lambda_1 v^2. \quad (2.22)$$

The fields H^\pm and A are the mass eigenstates and their masses are given by

$$m_{H^\pm}^2 = m_{22}^2 + \frac{\lambda_3}{2}v^2, \quad m_A^2 = m_{H^\pm}^2 + \frac{1}{2}(\lambda_4 - \lambda_5)v^2. \quad (2.23)$$

There is no mixing between h and H , which are the CP-even mass eigenstates

$$m_h^2 = \lambda_1 v^2 \equiv (125 \text{ GeV})^2, \quad m_H^2 = m_A^2 + \lambda_5 v^2. \quad (2.24)$$

The fermion masses can be obtained via the Yukawa interactions with Φ_1

$$-\mathcal{L} = y_u \bar{Q}_L \tilde{\Phi}_1 u_R + y_d \bar{Q}_L \Phi_1 d_R + y_l \bar{L}_L \Phi_1 e_R + \text{h.c.}, \quad (2.25)$$

where y_u , y_d and y_l are 3×3 matrices in family space. Because of the exact Z_2 symmetry, the inert field Φ_2 has no Yukawa interactions with fermions. The lightest neutral field, H or A , is stable and may be considered as a DM candidate. If right-handed neutrinos are introduced, then Φ_2 can interact with them, giving rise to the neutrino masses via the one loop with DM [76].

3 Constraints from theory and oblique parameters

3.1 Vacuum stability

Vacuum stability requires the potential to be bounded from below and stay positive for arbitrarily large values of the fields. The Higgs potential with a soft Z_2 symmetry breaking

term is given by

$$\begin{aligned}
V_{\text{tree}} = & m_{11}^2(\Phi_1^\dagger\Phi_1) + m_{22}^2(\Phi_2^\dagger\Phi_2) - \left[m_{12}^2(\Phi_1^\dagger\Phi_2 + \text{h.c.}) \right] \\
& + \frac{\lambda_1}{2}(\Phi_1^\dagger\Phi_1)^2 + \frac{\lambda_2}{2}(\Phi_2^\dagger\Phi_2)^2 + \lambda_3(\Phi_1^\dagger\Phi_1)(\Phi_2^\dagger\Phi_2) + \lambda_4(\Phi_1^\dagger\Phi_2)(\Phi_2^\dagger\Phi_1) \\
& + \left[\frac{\lambda_5}{2}(\Phi_1^\dagger\Phi_2)^2 + \text{h.c.} \right].
\end{aligned} \tag{3.1}$$

The fields can be parametrized as

$$\Phi_1^\dagger\Phi_1 = X_1^2, \quad \Phi_2^\dagger\Phi_2 = X_2^2, \quad \Phi_1^\dagger\Phi_2 = X_1X_2\rho e^{i\theta} \text{ with } 0 \leq \rho \leq 1. \tag{3.2}$$

For large values of the fields, the quadratic terms can be neglected and the quartic part is

$$V_4 = \frac{\lambda_1}{2}X_1^4 + \frac{\lambda_2}{2}X_2^4 + \lambda_3X_1^2X_2^2 + \lambda_4X_1^2X_2^2\rho^2 + \lambda_5X_1^2X_2^2\rho^2 \cos 2\theta. \tag{3.3}$$

After stabilizing θ at the minimum, we obtain the θ -independent part of potential

$$V_{\theta\text{-indep}} = \frac{\lambda_1}{2}X_1^4 + \frac{\lambda_2}{2}X_2^4 + \lambda_3X_1^2X_2^2 + \lambda_4X_1^2X_2^2\rho^2 - |\lambda_5|X_1^2X_2^2\rho^2. \tag{3.4}$$

For $\lambda_4 - |\lambda_5| > 0$, the potential has a minimal value at $\rho = 0$,

$$V_{\theta-\rho\text{-indep}} = \frac{\lambda_1}{2}X_1^4 + \frac{\lambda_2}{2}X_2^4 + \lambda_3X_1^2X_2^2. \tag{3.5}$$

For $\lambda_4 - |\lambda_5| < 0$, the potential has a minimal value at $\rho = 1$,

$$V_{\theta-\rho\text{-indep}} = \frac{\lambda_1}{2}X_1^4 + \frac{\lambda_2}{2}X_2^4 + \lambda_3X_1^2X_2^2 + \lambda_4X_1^2X_2^2 - |\lambda_5|X_1^2X_2^2. \tag{3.6}$$

Therefore, the vacuum stability requires

$$\lambda_1 > 0, \quad \lambda_2 > 0, \quad \lambda_3 + \sqrt{\lambda_1\lambda_2} > 0, \quad \lambda_3 + \lambda_4 - |\lambda_5| + \sqrt{\lambda_1\lambda_2} > 0. \tag{3.7}$$

In addition, there is the possibility that the 2HDM scalar potential of Eq. (3.1) has two minima, and the selected minimum is required to be global in order to avoid a metastable vacuum, which imposes the following condition [77],

$$m_{12}^2(m_{11}^2 - k^2m_{22}^2)(\tan\beta - k) > 0 \tag{3.8}$$

with $k = \sqrt[4]{\lambda_1/\lambda_2}$.

3.2 Unitarity

The amplitudes for scalar-scalar scattering $s_1s_2 \rightarrow s_3s_4$ at high energies respect unitarity [78]. A simple and explicit derivation can also be found in [79]. The starting point is the unitarity of the S matrix, $S = 1 + iT$,

$$SS^\dagger = 1 \longrightarrow T^\dagger T = -i(T - T^\dagger). \tag{3.9}$$

Then in terms of matrix elements of scattering from a pair of particles $a = 1, 2$ with momenta p_1, p_2 to a pair $b = 3, 4$ with momenta k_3, k_4 we have

$$\langle \{k, b\} | iT | \{p, a\} \rangle \equiv i \mathcal{M}_{ba} (2\pi)^4 \delta^4(k_3 + k_4 - p_1 - p_2). \quad (3.10)$$

We can obtain a bound on the partial wave

$$-\frac{i}{2}(a_J - a_J^\dagger) \geq a_J a_J^\dagger, \quad (3.11)$$

where a_J is a normal matrix related to the partial wave decomposition of $2 \rightarrow 2$ scattering matrix elements \mathcal{M}_{ba} ,

$$a_J^{\text{ba}} \equiv \frac{1}{32\pi} \sqrt{\frac{4|\mathbf{p}^b||\mathbf{p}^a|}{2\delta_{12}2\delta_{34}s}} \int_{-1}^1 d(\cos\theta) \mathcal{M}_{ba}(\cos\theta) P_J(\cos\theta). \quad (3.12)$$

The factor $\delta_{12}(\delta_{34})$ is 1 when the particles 1 and 2 (3 and 4) are identical, and zero otherwise. P_J are the Legendre polynomials, \mathbf{p}^i is the centre-of-mass three-momentum for particle i , and $s = (p_1 + p_2)^2$ is the standard Mandelstam variable.

We can diagonalize a and a^\dagger in Eq. (3.11) with an unitary matrix, and obtain the constraints on the eigenvalues (a_J^i):

$$\text{Im}(a_J^i) \geq |a_J^i|^2 \rightarrow [(\text{Re}(a_J^i))]^2 + \left[(\text{Im} a_J^i) - \frac{1}{2} \right]^2 \leq \frac{1}{4} \quad (3.13)$$

At tree-level, the bound is generally relaxed to

$$|\text{Re}(a_J^i)| \leq \frac{1}{2}. \quad (3.14)$$

We assume the external masses of $s_{1,2,3,4}$ are vanishing at high energy limit, and focus on the $J = 0$ partial wave. The modified zeroth partial wave for $s_1 s_2 \rightarrow s_3 s_4$ is

$$a_0 \simeq \frac{1}{16\pi} \left(2^{-\frac{1}{2}(\delta_{12} + \delta_{34})} Q_{1234} \right), \quad (3.15)$$

where Q_{1234} is quartic coupling of $s_1 s_2 s_3 s_4$.

Now we study the unitarity constraints on the 2HDM scalar potential. For the scalar potential in Eq. (3.1), one can take the uncoupled sets of scalar pairs

$$\{ \phi_1^+ \phi_2^-, \phi_1^- \phi_2^+, \phi_1 \phi_2, \phi_1 a_2, a_1 \phi_2, a_1 a_2 \}, \quad (3.16)$$

$$\{ \phi_1^+ \phi_1, \phi_1^+ a_1, \phi_2^+ \phi_2, \phi_2^+ a_2 \}, \quad (3.17)$$

$$\{ \phi_1^+ \phi_2, \phi_1^+ a_2, \phi_2^+ \phi_1, \phi_2^+ a_1 \}, \quad (3.18)$$

$$\{ \phi_1 a_1, \phi_2 a_2 \}, \quad (3.19)$$

$$\{ \phi_1^+ \phi_1^-, \phi_2^+ \phi_2^-, \phi_1 \phi_1, \phi_2 \phi_2, a_1 a_1, a_2 a_2 \} \quad (3.20)$$

to construct the matrix containing the tree-level amplitudes for $s_1 s_2 \rightarrow s_3 s_4$. We can obtain different eigenvalues of these matrices [80, 81]

$$a_{\pm} = \frac{3}{2}(\lambda_1 + \lambda_2) \pm \sqrt{\frac{9}{4}(\lambda_1 - \lambda_2)^2 + (2\lambda_3 + \lambda_4)^2}, \quad (3.21)$$

$$b_{\pm} = \frac{1}{2}(\lambda_1 + \lambda_2) \pm \sqrt{\frac{1}{4}(\lambda_1 - \lambda_2)^2 + \lambda_4^2}, \quad (3.22)$$

$$c_{\pm} = \frac{1}{2}(\lambda_1 + \lambda_2) \pm \sqrt{\frac{1}{4}(\lambda_1 - \lambda_2)^2 + \lambda_5^2}, \quad (3.23)$$

$$\mathbf{e}_{\pm} = \lambda_3 + 2\lambda_4 \pm 3\lambda_5, \quad (3.24)$$

$$\mathbf{f}_{\pm} = \lambda_3 \pm \lambda_4, \quad (3.25)$$

$$\mathbf{g}_{\pm} = \lambda_3 \pm \lambda_5. \quad (3.26)$$

The unitarity of the scattering process $s_1 s_2 \rightarrow s_3 s_4$ leads to

$$|a_{\pm}|, |b_{\pm}|, |c_{\pm}|, |\mathbf{e}_{\pm}|, |\mathbf{f}_{\pm}|, |\mathbf{g}_{\pm}| \leq 8\pi. \quad (3.27)$$

Here we stress that the conditions of Eq. (3.27) just indicate the approximate level above which the tree-level scattering amplitudes do not provide reliable results anymore. The problem is that we cannot rely on perturbative expansion when analyzing scattering, and therefore Eq. (3.27) is just our safety check, not the strict theory limitation. In addition, we take the standard approach to derive Eq. (3.15) and Eq. (3.27) and only consider quartic point-like couplings in the high energy limit. At finite energy, the additional diagrams of s , t , u channel in $s_1 s_2 \rightarrow s_3 s_4$ scattering can give some corrections to Eq. (3.15) and Eq. (3.27) [82].

3.3 Oblique parameters

The 2HDM can give additional contributions to gauge boson self-energies by the exchange of extra Higgs fields in the loops. The oblique parameters S , T and U were used to describe deviations of 2HDM from the SM, which are given as [83–85]

$$\begin{aligned} S = \frac{1}{\pi M_Z^2} & \left\{ \sin^2(\beta - \alpha) \left[\mathcal{B}_{22}(M_Z^2; M_Z^2, M_h^2) - M_Z^2 \mathcal{B}_0(M_Z^2; M_Z^2, M_h^2) + \mathcal{B}_{22}(M_Z^2; M_H^2, M_A^2) \right] \right. \\ & + \cos^2(\beta - \alpha) \left[\mathcal{B}_{22}(M_Z^2; M_Z^2, M_H^2) - M_Z^2 \mathcal{B}_0(M_Z^2; M_Z^2, M_H^2) + \mathcal{B}_{22}(M_Z^2; M_h^2, M_A^2) \right] \\ & \left. - \mathcal{B}_{22}(M_Z^2; M_{H^\pm}^2, M_{H^\pm}^2) - \mathcal{B}_{22}(M_Z^2; M_Z^2, M_{h,\text{ref}}^2) + M_Z^2 \mathcal{B}_0(M_Z^2; M_Z^2, M_{h,\text{ref}}^2) \right\}, \quad (3.28) \end{aligned}$$

$$\begin{aligned} T = \frac{1}{16\pi M_W^2 s_W^2} & \left\{ \sin^2(\beta - \alpha) \left[\mathcal{F}(M_{H^\pm}^2, M_H^2) - \mathcal{F}(M_H^2, M_A^2) + 3\mathcal{F}(M_Z^2, M_h^2) - 3\mathcal{F}(M_W^2, M_h^2) \right] \right. \\ & + \cos^2(\beta - \alpha) \left[\mathcal{F}(M_{H^\pm}^2, M_h^2) - \mathcal{F}(M_h^2, M_A^2) + 3\mathcal{F}(M_Z^2, M_H^2) - 3\mathcal{F}(M_W^2, M_H^2) \right] \\ & \left. + \mathcal{F}(M_{H^\pm}^2, M_A^2) - 3\mathcal{F}(M_Z^2, M_{h,\text{ref}}^2) + 3\mathcal{F}(M_W^2, M_{h,\text{ref}}^2) \right\} \quad (3.29) \end{aligned}$$

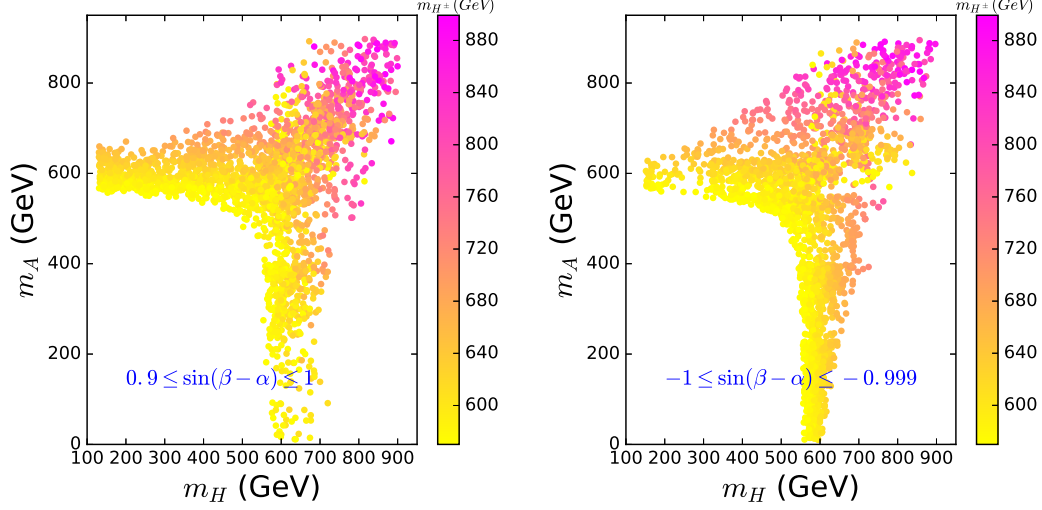


Figure 1. Scatter plots of m_A and m_H satisfying the constraints of vacuum stability, unitarity, perturbativity, and the oblique parameters for $570 \text{ GeV} \leq m_{H^\pm} \leq 900 \text{ GeV}$, taken from [87].

$$\begin{aligned}
U &= \mathcal{H}(M_W^2) - \mathcal{H}(M_Z^2) \\
&+ \frac{1}{\pi M_W^2} \left\{ \cos^2(\beta - \alpha) \mathcal{B}_{22}(M_W^2; M_{H^\pm}^2, M_h^2) + \sin^2(\beta - \alpha) \mathcal{B}_{22}(M_W^2; M_{H^\pm}^2, M_H^2) \right. \\
&+ \left. \mathcal{B}_{22}(M_W^2; M_{H^\pm}^2, M_A^2) - 2 \mathcal{B}_{22}(M_W^2; M_{H^\pm}^2, M_{H^\pm}^2) \right\} \\
&- \frac{1}{\pi M_Z^2} \left\{ \cos^2(\beta - \alpha) \mathcal{B}_{22}(M_Z^2; M_h^2, M_A^2) + \sin^2(\beta - \alpha) \mathcal{B}_{22}(M_Z^2; M_H^2, M_A^2) \right. \\
&- \left. \mathcal{B}_{22}(M_Z^2; M_{H^\pm}^2, M_{H^\pm}^2) \right\}, \tag{3.30}
\end{aligned}$$

where

$$\begin{aligned}
\mathcal{H}(M_V^2) &\equiv \frac{1}{\pi M_V^2} \left\{ \sin^2(\beta - \alpha) \left[\mathcal{B}_{22}(M_V^2; M_V^2, M_h^2) - M_V^2 \mathcal{B}_0(M_V^2; M_V^2, M_h^2) \right] \right. \\
&+ \cos^2(\beta - \alpha) \left[\mathcal{B}_{22}(M_V^2; M_V^2, M_H^2) - M_V^2 \mathcal{B}_0(M_V^2; M_V^2, M_H^2) \right] \\
&- \left. \mathcal{B}_{22}(M_V^2; M_V^2, M_{h,\text{ref}}^2) + M_V^2 \mathcal{B}_0(M_V^2; M_V^2, M_{h,\text{ref}}^2) \right\}. \tag{3.31}
\end{aligned}$$

The loop functions are given by

$$\begin{aligned}
B_{22}(q^2; m_1^2, m_2^2) &= \frac{1}{4}(\Delta + 1) [m_1^2 + m_2^2 - \frac{1}{3}q^2] - \frac{1}{2} \int_0^1 dx X \log(X - i\epsilon), \\
B_0(q^2; m_1^2, m_2^2) &= \Delta - \int_0^1 dx \log(X - i\epsilon), \\
\mathcal{F}(m_1^2, m_2^2) &= \frac{1}{2}(m_1^2 + m_2^2) - \frac{m_1^2 m_2^2}{m_1^2 - m_2^2} \log\left(\frac{m_1^2}{m_2^2}\right),
\end{aligned} \tag{3.32}$$

where

$$X \equiv m_1^2 x + m_2^2 (1 - x) - q^2 x(1 - x), \quad \Delta \equiv \frac{2}{4 - d} + \ln 4\pi - \gamma_E, \tag{3.33}$$

in d space-time dimensions. The \mathcal{B}_{22} and \mathcal{B}_0 functions are defined as

$$\mathcal{B}_{22}(q^2; m_1^2, m_2^2) \equiv B_{22}(q^2; m_1^2, m_2^2) - B_{22}(0; m_1^2, m_2^2), \tag{3.34}$$

$$\mathcal{B}_0(q^2; m_1^2, m_2^2) \equiv B_0(q^2; m_1^2, m_2^2) - B_0(0; m_1^2, m_2^2). \tag{3.35}$$

The above expressions show that the oblique parameters S , T and U are sensitive to the mass splitting of extra Higgs bosons. If h is taken as the 125 GeV Higgs, H or A is favored to have small mass splitting from H^\pm . Fig. 1 shows m_H and m_A for type-II 2HDM allowed by the global fit values to the oblique parameters [86],

$$S = 0.02 \pm 0.10, \quad T = 0.07 \pm 0.12, \quad U = 0.00 \pm 0.09, \tag{3.36}$$

with correlation coefficients

$$\rho_{ST} = 0.89, \quad \rho_{SU} = -0.54, \quad \rho_{TU} = -0.83. \tag{3.37}$$

In Fig. 1 $m_{H^\pm} > 570$ GeV is taken to satisfy the constraints of the experimental data of $b \rightarrow s\gamma$ [88].

Very recently the CDF collaboration reported their new result for the W -boson mass measurement [55]

$$m_W = 80.4335 \pm 0.0094 \text{ GeV}, \tag{3.38}$$

which has an approximate 7σ deviation from the SM prediction, $m_W(\text{SM}) = 80.357 \pm 0.006$ GeV [89]. The shifted W -mass modifies the global fit values to S , T , and U [90]

$$S = 0.06 \pm 0.10, \quad T = 0.11 \pm 0.12, \quad U = 0.14 \pm 0.09, \tag{3.39}$$

with correlation coefficients

$$\rho_{ST} = 0.9, \quad \rho_{SU} = -0.59, \quad \rho_{TU} = -0.85. \tag{3.40}$$

The W -boson mass can be inferred from the following relation [91],

$$m_W^2 = m_W^2(\text{SM}) + \frac{\alpha c_W^2}{c_W^2 - s_W^2} m_Z^2 \left(-\frac{1}{2} S + c_W^2 T + \frac{c_W^2 - s_W^2}{4s_W^2} U \right). \quad (3.41)$$

In the 2HDM, the correction to T is usually larger than S and U . In order to accommodate the W -mass reported by the CDF II collaboration, the 2HDM needs to give an appropriate value of T . Therefore, H/A is disfavored to degenerate in mass with H^\pm . Various types of 2HDMs have been used to explain the W -mass [56–69]. Ref. [59] discussed the CDF W -mass in the 2HDM with an exact Z_4 symmetry and found that the CDF W -mass favors the mass splitting between H^\pm and H/A to be larger than 10 GeV, and allows H and A to degenerate. The m_{H^\pm} and m_A are favored to be smaller than 650 GeV for $m_H < 120$ GeV, and allowed to have more large values with increasing of m_H .

4 Constraints from LHC searches for Higgs bosons

4.1 Signal data of the 125 GeV Higgs

In the four types of 2HDMs, the neutral Higgs Yukawa couplings normalized to the SM are given by

$$y_h^{fi} = [\sin(\beta - \alpha) + \cos(\beta - \alpha)\kappa_f], \quad (4.1)$$

$$y_H^{fi} = [\cos(\beta - \alpha) - \sin(\beta - \alpha)\kappa_f], \quad (4.2)$$

$$y_A^{fi} = -i\kappa_f \text{ (for u)}, \quad (4.3)$$

$$y_A^{fi} = i\kappa_f \text{ (for d, } \ell). \quad (4.4)$$

The neutral Higgs couplings with gauge bosons normalized to the SM are

$$y_h^V = \sin(\beta - \alpha), \quad y_H^V = \cos(\beta - \alpha), \quad (4.5)$$

with V denoting W or Z .

The analyses of ATLAS and CMS collaborations show that the coupling strengths of the discovered 125 GeV boson agree well with the SM Higgs boson, but the sign of the couplings cannot be measured directly. If we take h as the 125 GeV Higgs boson, its couplings have two different cases:

$$y_h^{fi} \times y_h^V > 0 \quad \text{(for SM-like couplings)}, \quad (4.6)$$

$$y_h^{fi} \times y_h^V < 0 \quad \text{(for wrong-sign Yukawa couplings)}. \quad (4.7)$$

In the case of the SM-like couplings, the couplings of the 125 GeV Higgs are very close to those in the SM, which has an alignment limit. In the exact alignment limit [92, 93], namely $\cos(\beta - \alpha) = 0$, from Eq. (4.1) and Eq. (4.5) we see that h has the same couplings to the fermions and gauge bosons as in the SM, and the heavy CP-even Higgs H has no couplings to the gauge bosons.

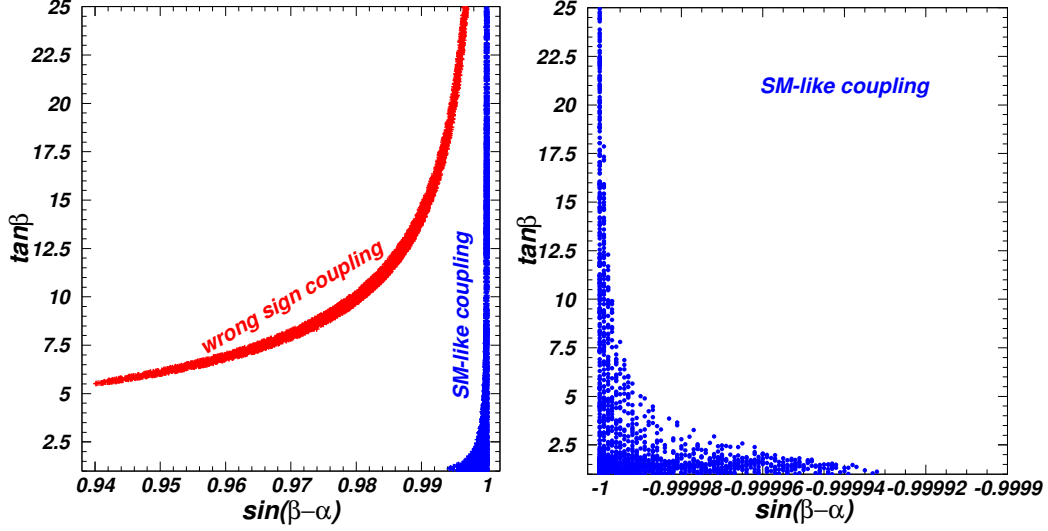


Figure 2. Scatter plots of $\sin(\beta - \alpha)$ and $\tan\beta$ of type-II model satisfying the constraints of the 125 GeV Higgs signal data, taken from [113].

Now we discuss the wrong-sign Yukawa couplings [87, 94–98, 100–110]. The signal data of the 125 GeV Higgs require the absolute values of $y_h^{f_i}$ and y_h^V to be close to 1.0. Thus, we approximately express $y_h^{f_i}$ and y_h^V with ϵ and $\cos(\beta - \alpha)$ as

$$y_h^{f_i} = -1 + \epsilon, \quad y_h^V \simeq 1 - 0.5 \cos^2(\beta - \alpha) \quad \text{for } \sin(\beta - \alpha) > 0 \text{ and } \cos(\beta - \alpha) > 0, \quad (4.8)$$

$$y_h^{f_i} = 1 - \epsilon, \quad y_h^V \simeq -1 + 0.5 \cos^2(\beta - \alpha) \quad \text{for } \sin(\beta - \alpha) < 0 \text{ and } \cos(\beta - \alpha) > 0. \quad (4.9)$$

From Eq. (4.1) we can get

$$\kappa_f = \frac{-2 + \epsilon + 0.5 \cos(\beta - \alpha)^2}{\cos(\beta - \alpha)} \ll -1 \quad \text{for } \sin(\beta - \alpha) > 0 \text{ and } \cos(\beta - \alpha) > 0, \quad (4.10)$$

$$\kappa_f = \frac{2 - \epsilon - 0.5 \cos(\beta - \alpha)^2}{\cos(\beta - \alpha)} \gg 1 \quad \text{for } \sin(\beta - \alpha) < 0 \text{ and } \cos(\beta - \alpha) > 0. \quad (4.11)$$

In the four types of 2HDMs, the measurement of the branching fraction of $b \rightarrow s\gamma$ favors a $\tan\beta$ greater than 1. Therefore, for $\sin(\beta - \alpha) > 0$ and $\cos(\beta - \alpha) > 0$, there may exist wrong-sign Yukawa couplings for the down-type quarks and leptons in the type-II model, for the leptons in the L2HDM, and for the down-type quarks in the flipped 2HDM.

Fig. 2 shows $\sin(\beta - \alpha)$ and $\tan\beta$ of type-II model allowed by the 125 GeV Higgs signal data. The value of $\sin(\beta - \alpha)$ in the case of the wrong-sign Yukawa couplings is allowed to deviate from 1 more sizably than in the case of the SM-like couplings. In the case of the wrong-sign Yukawa couplings, $\tan\beta$ has stringent upper and lower bounds for a given value of $\sin(\beta - \alpha)$.

Table 3. The upper limits at 95% C.L. on the production cross section times branching ratio for the channels of H and A searches at the LHC.

Channel	Experiment	Mass range [GeV]	Luminosity
$gg/b\bar{b} \rightarrow H/A \rightarrow \tau^+\tau^-$	CMS 13 TeV [114]	200-2250	36.1 fb ⁻¹
$gg/b\bar{b} \rightarrow H/A \rightarrow \tau^+\tau^-$	ATLAS 13 TeV [115]	200-2500	139 fb ⁻¹
$gg \rightarrow H/A \rightarrow t\bar{t}$	CMS 13 TeV [116]	400-750	35.9 fb ⁻¹
$gg \rightarrow H/A \rightarrow \gamma\gamma + t\bar{t}H/A (H/A \rightarrow \gamma\gamma)$	CMS 13 TeV [117]	70-110	35.9 fb ⁻¹
$VV \rightarrow H \rightarrow \gamma\gamma + VH (H \rightarrow \gamma\gamma)$	CMS 13 TeV [117]	70-110	35.9 fb ⁻¹
$gg/VV \rightarrow H \rightarrow W^+W^- (\ell\nu qq)$	ATLAS 13 TeV [118]	200-3000	36.1 fb ⁻¹
$gg/VV \rightarrow H \rightarrow W^+W^- (e\nu\mu\nu)$	ATLAS 13 TeV [119]	200-3000	36.1 fb ⁻¹
$gg/VV \rightarrow H \rightarrow W^+W^-$	CMS 13 TeV [120]	200-3000	35.9 fb ⁻¹
$gg/VV \rightarrow H \rightarrow ZZ$	ATLAS 13 TeV [121]	200-2000	36.1 fb ⁻¹
$gg/VV \rightarrow H \rightarrow ZZ$	ATLAS 13 TeV [122]	300-5000	36.1 fb ⁻¹
$gg/VV \rightarrow H \rightarrow ZZ$	ATLAS 13 TeV [123]	200-2000	139 fb ⁻¹
$gg \rightarrow H \rightarrow hh \rightarrow b\bar{b}b\bar{b}$	CMS 13 TeV [124]	750-3000	35.9 fb ⁻¹
$gg \rightarrow H \rightarrow hh \rightarrow (b\bar{b})(\tau^+\tau^-)$	CMS 13 TeV [125]	250-900	35.9 fb ⁻¹
$pp \rightarrow H \rightarrow hh$	CMS 13 TeV [126]	250-3000	35.9 fb ⁻¹
$gg \rightarrow H \rightarrow hh \rightarrow b\bar{b}ZZ$	CMS 13 TeV [127]	260-1000	35.9 fb ⁻¹
$gg \rightarrow H \rightarrow hh \rightarrow b\bar{b}\tau^+\tau^-$	CMS 13 TeV [128]	1000-3000	139 fb ⁻¹
$gg/b\bar{b} \rightarrow A \rightarrow hZ \rightarrow (b\bar{b})Z$	ATLAS 13 TeV [129]	200-2000	36.1 fb ⁻¹
$gg/b\bar{b} \rightarrow A \rightarrow hZ \rightarrow (b\bar{b})Z$	CMS 13 TeV [130]	225-1000	35.9 fb ⁻¹
$gg \rightarrow A \rightarrow hZ \rightarrow (\tau^+\tau^-)(\ell\ell)$	CMS 13 TeV [131]	220-400	35.9 fb ⁻¹
$gg/b\bar{b} \rightarrow A(H) \rightarrow H(A)Z \rightarrow (b\bar{b})(\ell\ell)$	ATLAS 13 TeV [132]	130-800	36.1 fb ⁻¹
$gg \rightarrow A(H) \rightarrow H(A)Z \rightarrow (b\bar{b})(\ell\ell)$	CMS 13 TeV [133]	30-1000	35.9 fb ⁻¹

4.2 Searches for additional scalars at LHC

The ATLAS and CMS collaborations have searched for an additional scalar from its decay into various SM channels or from its exotic decays. Since the Yukawa couplings of down-type quarks and leptons can be both enhanced by a factor of $\tan\beta$, the type-II model can be more stringently constrained than other three types of models by the flavor observables and the LHC searches for additional Higgs.

At the LHC, the dominant production processes of H and A are from the gluon-gluon fusions, which are generated by exchanging top quark and b -quark in the loops. There may be destructive interference between contributions of b -quark loop and top quark loop. The SusHi [111] was used to calculate the cross sections for H and A in the gluon fusion and $b\bar{b}$ -associated production at NNLO in QCD, while the 2HDMC was employed to precisely calculate the branching ratios of the various decay modes of H and A [112].

The studies in [87, 113] used a large number of ATLAS and CMS analyses at the 8 TeV and 13 TeV LHC to constrain the type-II 2HDM. Table 3 lists some analyses at the 13 TeV LHC with more than 35.9 fb⁻¹ integrated luminosity data. Fig. 3 shows the surviving samples with the SM-like coupling of type-II model satisfying various LHC direct searches. The couplings of AhZ and AHZ are respectively proportional to $\cos(\beta - \alpha)$ and $\sin(\beta - \alpha)$. For the case of the SM-like coupling, $|\sin(\beta - \alpha)|$ is very closed to 1. Therefore, the $A \rightarrow hZ$

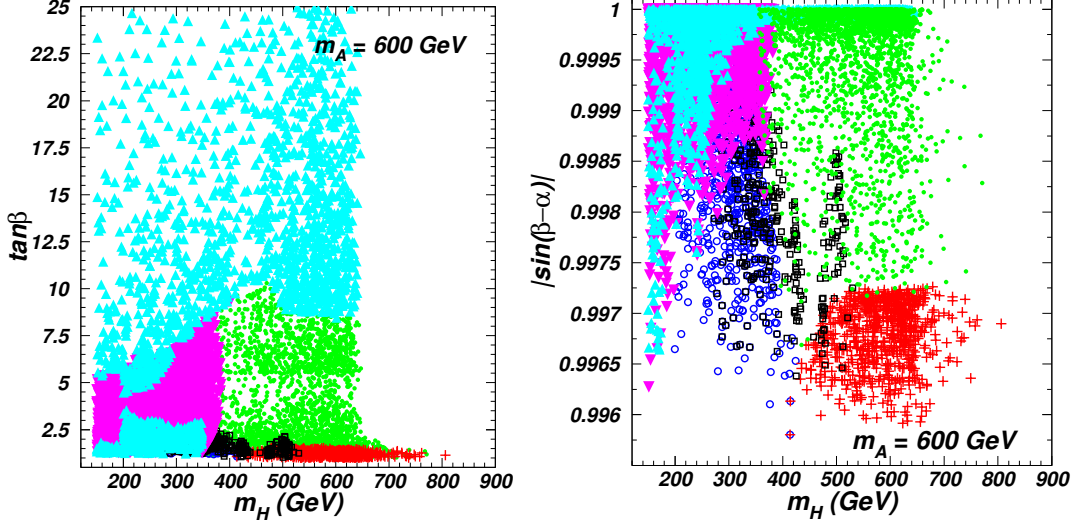


Figure 3. The surviving samples with the SM-like couplings of type-II model, taken from [113]. The triangles (sky blue), circles (royal blue), squares (black), inverted triangles (purple), and pluses (red) are respectively excluded by the $H/A \rightarrow \tau^+\tau^-$, $H \rightarrow WW, ZZ, \gamma\gamma$, $H \rightarrow hh$, $A \rightarrow HZ$, and $A \rightarrow hZ$ channels at the LHC. The bullets (green) samples are allowed by various LHC direct searches.

channel fails to constrain the parameter space, and the $A \rightarrow HZ$ channel can exclude many points in the region of $m_H < 360$ GeV. The $H/A \rightarrow \tau^+\tau^-$ channels give upper bound on $\tan\beta$, and allow m_H to vary from 150 GeV to 800 GeV for appropriate $\tan\beta$ and $\sin(\beta - \alpha)$. Fig. 3 shows the joint constraints of $H/A \rightarrow \tau^+\tau^-$, $A \rightarrow HZ$, $H \rightarrow WW, ZZ, \gamma\gamma$, and $H \rightarrow hh$ exclude the whole region of $m_H < 360$ GeV.

The surviving samples with the wrong-sign Yukawa couplings of type-II model are shown in Fig. 4. For the case of the wrong-sign Yukawa couplings, the signal data of the 125 GeV Higgs requires $\tan\beta > 5$ and allows $\sin(\beta - \alpha)$ to be as low as 0.94, as shown in Fig. 2. As a result, the cross sections of H and A in the gluon fusion productions are sizably suppressed, and only $b\bar{b} \rightarrow A \rightarrow \tau^+\tau^-$ and $A \rightarrow hZ$ channels can be used to constrain the parameter space. Especially for $m_H = 600$ GeV, the constraints are very stringent, and the allowed samples are mainly distributed in several corners. Many samples with m_A in the ranges of $30 \sim 120$ GeV, $240 \sim 300$ GeV, $380 \sim 430$ GeV, and $480 \sim 550$ GeV are allowed for appropriate $\tan\beta$ and $\sin(\beta - \alpha)$. Also the samples in the regions of $m_A < 20$ GeV and $80 \text{ GeV} < m_A < 90$ GeV are allowed since there is no experimental data of $A \rightarrow \tau^+\tau^-$ channel in these ranges.

For the case of $m_A = 600$ GeV, the constraints of the $b\bar{b} \rightarrow A \rightarrow \tau^+\tau^-$ and $A \rightarrow hZ$ channels can be relatively relaxed. Many samples of $150 \text{ GeV} < m_H < 470$ GeV are allowed and $m_H > 470$ GeV is excluded. For a small m_H , the $A \rightarrow HZ$ decay will open and increase the total width of A . As a result, the branching ratio of $A \rightarrow hZ$ can be sizably suppressed, and weaken the constraints of the $A \rightarrow hZ$ channel.

Compared to the type-II 2HDM, all the Yukawa couplings of H , A and H^\pm in the type-I

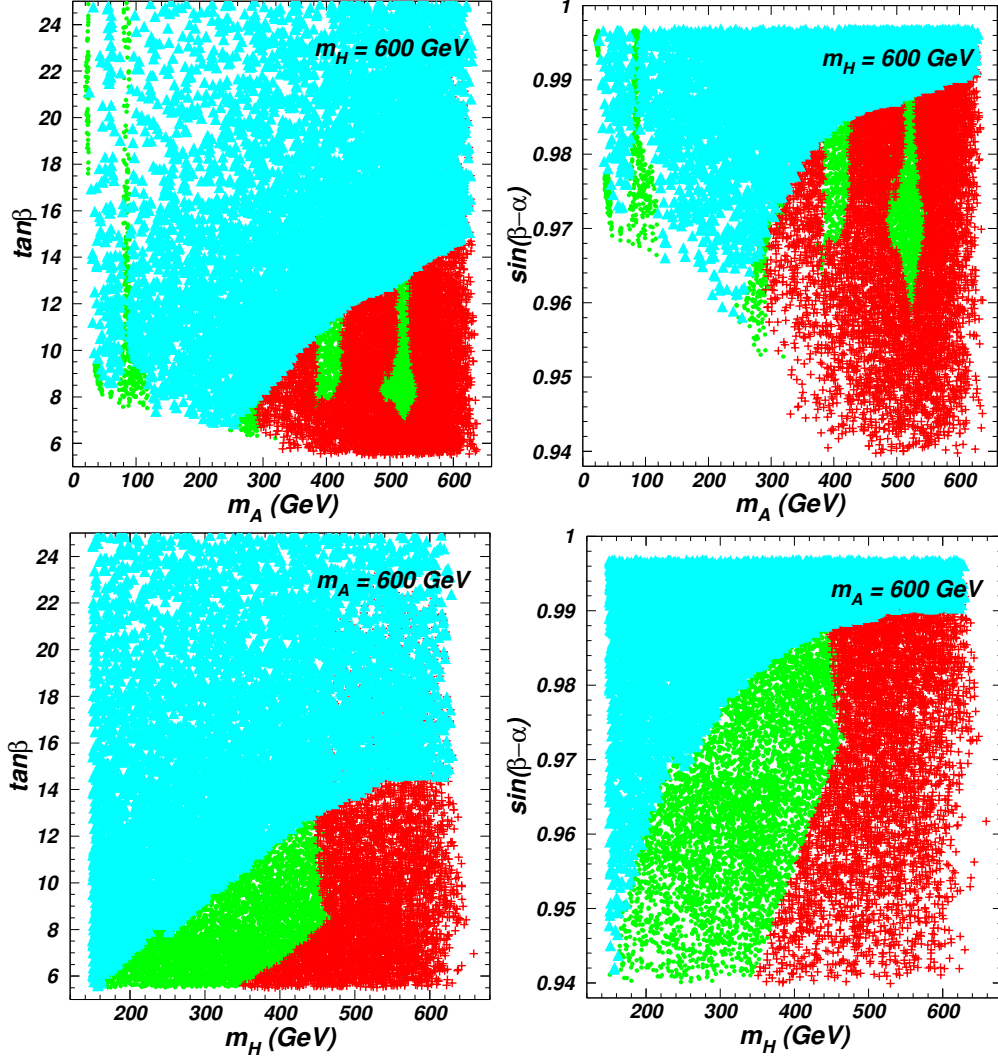


Figure 4. The surviving samples with the wrong-sign Yukawa couplings of type-II model, taken from [87]. The triangles (sky blue) and pluses (red) are respectively excluded by the $A/H \rightarrow \tau^+\tau^-$ and $A \rightarrow hZ$ channels at the LHC. The bullets (green) are allowed by various LHC direct searches.

model can be suppressed by a large $\tan \beta$, which leads that the searches for additional scalars at the LHC and measurements of the flavor observables are easily satisfied. Thus, H , A and H^\pm are allowed to have broad mass ranges. There are some recent studies on the status of type-I and type-II 2HDMs confronted with the direct searches at the LHC, see, e.g., [134–144].

5 Dark matter observables

5.1 Inert 2HDM and dark matter

Because of the exact Z_2 symmetry, the lightest neutral component H or A is stable and may be considered as a DM candidate. If taking H as the DM, it requires

$$\lambda_5 < 0, \quad \lambda_4 - |\lambda_5| < 0. \quad (5.1)$$

Flipping the sign of λ_5 , A will be the DM candidate. The parameter $\lambda_{345} = \lambda_3 + \lambda_4 + \lambda_5$ controls the hHH coupling, which will affect the signal strengths of the 125 GeV Higgs and the DM observables.

The main possible annihilation channels include $HH \rightarrow f\bar{f}$, $VV^{(*)}$, hh and various co-annihilations of the inert scalars. In addition to the constraints from theory and the oblique parameters as well as the signal data of the 125 GeV Higgs, the model should also satisfy the precise measurements of the W and Z widths, which requires

$$m_A + m_H > m_Z, \quad 2m_{H^\pm} > m_Z, \quad m_A + m_{H^\pm} > m_W, \quad m_H + m_{H^\pm} > m_W. \quad (5.2)$$

The null searches at the LEP exclude two regions [145, 146],

$$m_{H^\pm} < 70\text{GeV}, \quad (5.3)$$

$$m_H < 80\text{ GeV}, \quad m_A < 100\text{ GeV}, \quad \text{and} \quad m_A - m_H > 8\text{GeV}. \quad (5.4)$$

Considering various relevant theoretical and experimental constraints, the allowed DM mass ranges have been discussed, see e.g. [147–158]. Because of the tension between the signal strength of the 125 GeV Higgs and the relic density, $m_H < 55$ GeV is disfavored. In the resonance region of $m_H \simeq \frac{m_h}{2}$, the main annihilation channels are h -mediated, primarily into $b\bar{b}$ and WW final states. The correct relic density can be obtained and the relevant constraints can be satisfied. In the region up to around 75 GeV, the HH pair mainly annihilates to WW^* via the processes mediated by h or via the quartic couplings. Under the relevant constraints, the correct relic density can be rendered for $73\text{ GeV} < m_H < 75\text{ GeV}$. For $75\text{ GeV} < m_H < 160\text{ GeV}$, the correct relic density requires λ_{345} to be large enough to lead to an appropriate cancelation between diagrams of VV^* . However, such a large λ_{345} is excluded by the DM direct detections. In the region between 160 GeV and 500 GeV, the annihilation cross section of $HH \rightarrow W^+W^-$ is too large to produce the exact relic density. In the region of $m_H > 500\text{ GeV}$, the exact relic density favors small mass splittings among the three inert Higgs bosons, roughly $\leq 10\text{ GeV}$. The large mass splittings tend to enhance the cross section of HH annihilation into longitudinal Z and W bosons.

5.2 Wrong-sign Yukawa couplings and isospin-violating interactions between dark matter and nucleons.

Although the inert 2HDM may provide a DM candidate, but its mass range is stringently constrained. Alternatively, a real singlet scalar DM can be added to the 2HDM, and this

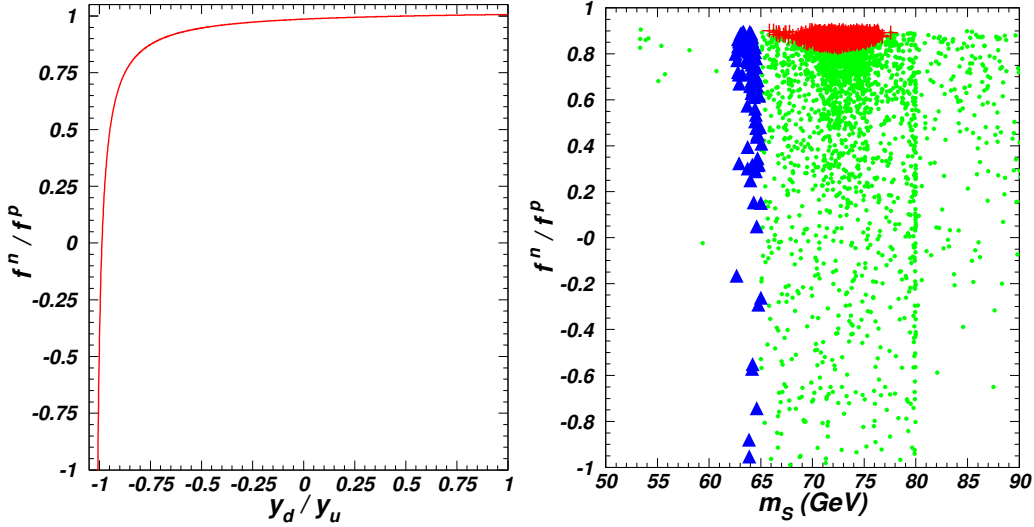


Figure 5. Left: f^n/f^p versus y_d/y_u with y_d (y_u) denoting the Yukawa coupling of $h d \bar{d}$ ($h u \bar{u}$) normalized to the SM value [42]. Right: All the samples are allowed by the constraints of the LHC searches and the DM relic density. The pluses (red) are excluded by the constraints of the spin-independent DM-proton cross section from XENON1T (2017), and the triangles (royal blue) are excluded by the Fermi-LAT search for DM annihilation from dSphs [42].

DM has different properties from the DM in inert 2HDM. Especially for the type-II 2HDM, the 125 GeV Higgs may have wrong-sign Yukawa couplings with down-type quarks. If such a Higgs acts as the portal between the DM and SM sectors, the model can give the isospin-violating interactions between DM and nucleons, which can relax the constraints from the DM direct detections.

A real singlet scalar S is introduced to the type-II 2HDM under a Z'_2 symmetry in which $S \rightarrow -S$. The potential containing the S field is written as [35]

$$\mathcal{V}_S = \frac{1}{2} S^2 (\kappa_1 \Phi_1^\dagger \Phi_1 + \kappa_2 \Phi_2^\dagger \Phi_2) + \frac{m_0^2}{2} S^2 + \frac{\lambda_S}{4!} S^4. \quad (5.5)$$

The S field has no vev and may serve as a DM candidate. The DM mass and the cubic interactions with the neutral Higgs bosons are obtained from Eq. (5.5),

$$m_S^2 = m_0^2 + \frac{1}{2} \kappa_1 v^2 \cos^2 \beta + \frac{1}{2} \kappa_2 v^2 \sin^2 \beta, \quad (5.6)$$

$$-\lambda_h v S^2 h/2 \equiv -(-\kappa_1 \sin \alpha \cos \beta + \kappa_2 \cos \alpha \sin \beta) v S^2 h/2, \quad (5.7)$$

$$-\lambda_H v S^2 H/2 \equiv -(\kappa_1 \cos \alpha \cos \beta + \kappa_2 \sin \alpha \sin \beta) v S^2 H/2. \quad (5.8)$$

In this model, the elastic scattering of S on a nucleon receives the contributions from the process with t -channel exchange of h and H . The spin-independent cross section is written as [159],

$$\sigma_{p(n)} = \frac{\mu_{p(n)}^2}{4\pi m_S^2} \left[f^{p(n)} \right]^2, \quad (5.9)$$

where $\mu_{p(n)} = \frac{m_S m_{p(n)}}{m_S + m_{p(n)}}$ and

$$f^{p(n)} = \sum_{q=u,d,s} f_q^{p(n)} \mathcal{C}_{Sq} \frac{m_{p(n)}}{m_q} + \frac{2}{27} f_g^{p(n)} \sum_{q=c,b,t} \mathcal{C}_{Sq} \frac{m_{p(n)}}{m_q}, \quad (5.10)$$

with $\mathcal{C}_{Sq} = \frac{\lambda_h}{m_h^2} m_q y_q^h + \frac{\lambda_H}{m_H^2} m_q y_q^H$. Here f_q^p (f_q^n) is the form factor at the proton (neutron) for a light quark q , and f_g^p (f_g^n) is the form factor at the proton (neutron) for gluon [160],

$$\begin{aligned} f_u^p &\approx 0.0208, & f_d^p &\approx 0.0399, & f_s^p &\approx 0.0430, & f_g^p &\approx 0.8963, \\ f_u^n &\approx 0.0188, & f_d^n &\approx 0.0440, & f_s^n &\approx 0.0430, & f_g^n &\approx 0.8942. \end{aligned} \quad (5.11)$$

A simple scenario is to take the 125 GeV Higgs (h) as the only portal between the DM and SM sectors. If $f_q^p \neq f_q^n$, the S -nucleon scattering may be isospin-violating for the appropriate values of y_h^d and y_h^u .

The left panel of Fig. 5 shows that f^n/f^p approaches to 1 with y_d/y_u . Namely, the S -nucleon scattering is isospin-conserving for $y_d = y_u$ and significantly isospin-violating when y_d/y_u deviates from 1 sizably, especially that there is an opposite sign between y_d and y_u . The right panel shows that the bounds of the direct detection experiments can be satisfied in the region $-1 < f^n/f^p < 0.8$. The DM scattering rate with Xe target can be sizably suppressed for $f^n/f^p \sim -0.7$, which can weaken the constraints from the spin-independent DM-nucleon cross section.

There are other DM extensions of 2HDM which accomodate the DM direct detection limits. In the general 2HDM with a DM, when both h and H are portals between the SM sector and DM, and have appropriate couplings, the model can achieve the blind spots at DM direct detection, which originates from cancellations between interfering diagrams with h and H exchanges [47, 48]. Besides, in the L2HDM with a DM, the quark Yukawa couplings of H can be significantly suppressed for a very large $\tan\beta$. If such a H field is taken as the portal between the SM sector and DM, the model can easily weaken the bound of the DM direct detection and explain the muon $g-2$ [49, 50].

6 Muon anomalous magnetic moment

6.1 L2HDM and muon $g-2$

The muon $g-2$ is a very precisely measured observable and serves as a sensitive probe of new physics (for a pedagogical review, see, e.g., [161]). The new Fermilab measurement [162] combined with E821 data [163] shows a 4.2σ deviation from the SM prediction [164–167]. Such a discrepancy has been explained in various new physics models like the minimal supersymmetry (see, e.g., [168–171]). Among the 2HDMs, the L2HDM can offer an explanation.

In the L2HDM, the lepton (quark) Yukawa couplings to H , A and H^\pm can be sizably enhanced (suppressed) by a large $\tan\beta$. The model has been extensively studied to explain the muon $g-2$, and the searches at the LHC and low energy precision measurements can exclude

a large part of parameter space for the explanation of muon $g-2$. The study in [19] considered the signal data of the 125 GeV Higgs, and found that the muon $g-2$ explanation favors the 125 GeV Higgs to have wrong-sign Yukawa couplings to the leptons. The experimental results of $\text{Br}(B_s \rightarrow \mu^+ \mu^-)$ can exclude some parameter regions with a very light A [19]. Besides, the measurements of lepton flavor universality (LFU) of the Z decays and τ decays give stringent constraints on $\tan \beta$ and the mass splittings among H , A and H^\pm [20, 24], and a more precise study was performed in [23]. The muon $g-2$ explanation makes the additional Higgs bosons to have τ -rich signatures at the LHC, and the study in [21] first used the chargino/neutralino searches at the 8 TeV LHC to constrain the model. The analysis in [27] used the constraints of the multi-lepton analyses at the 13 TeV, and found that the L2HDM may explain the muon $g-2$ anomaly and produce a strong first order electroweak phase transition (SFOEWPT) simultaneously.

In the L2HDM, the additional contributions to the muon $g-2$ are mainly from the one-loop diagrams and the two-loop Barr-Zee diagrams mediated by A , H and H^\pm . The one-loop contributions is given by [172–174]

$$\Delta a_\mu^{\text{2HDM}}(1\text{-loop}) = \frac{G_F m_\mu^2}{4\pi^2 \sqrt{2}} \sum_j (y_\mu^j)^2 r_\mu^j f_j(r_\mu^j), \quad (6.1)$$

where $j = H, A, H^\pm$, $r_\mu^j = m_\mu^2/M_j^2$. For $r_\mu^j \ll 1$ we have

$$f_H(r) \simeq -\ln r - 7/6, \quad f_A(r) \simeq \ln r + 11/6, \quad f_{H^\pm}(r) \simeq -1/6. \quad (6.2)$$

For the main two-loop contributions, we have

$$\Delta a_\mu^{\text{2HDM}}(2\text{-loop}) = \frac{G_F m_\mu^2}{4\pi^2 \sqrt{2}} \frac{\alpha_{\text{em}}}{\pi} \sum_{i,f} N_f^c Q_f^2 y_\mu^i y_f^i r_f^i g_i(r_f^i), \quad (6.3)$$

where $i = H, A$, and m_f, Q_f and N_f^c are the mass, electric charge and the number of color degrees of freedom of the fermion f in the loop. The functions $g_i(r)$ are given by [175–177]

$$g_{h,H}(r) = \int_0^1 dx \frac{2x(1-x) - 1}{x(1-x) - r} \ln \frac{x(1-x)}{r}, \quad (6.4)$$

$$g_A(r) = \int_0^1 dx \frac{1}{x(1-x) - r} \ln \frac{x(1-x)}{r}. \quad (6.5)$$

The contributions of H and A to Δa_μ are positive (negative) at one-loop level and negative (positive) at the two-loop level. Since m_f^2/m_μ^2 easily overcomes the loop suppression factor α/π , the two-loop contributions can be larger than one-loop ones. As a result, the L2HDM can enhance the value of Δa_μ for $m_A < m_H$. In [178] the authors presented an extension of the GM2Calc software to calculate the muon $g-2$ of 2HDM precisely.

Because of the large lepton Yukawa couplings, the L2HDM can give sizable corrections to the Z and τ decays, and thus be constrained by the measured values of LFU of the Z -boson

[179]

$$\frac{\Gamma_{Z \rightarrow \mu^+ \mu^-}}{\Gamma_{Z \rightarrow e^+ e^-}} = 1.0009 \pm 0.0028, \quad (6.6)$$

$$\frac{\Gamma_{Z \rightarrow \tau^+ \tau^-}}{\Gamma_{Z \rightarrow e^+ e^-}} = 1.0019 \pm 0.0032, \quad (6.7)$$

and τ decays [180],

$$\begin{aligned} \left(\frac{g_\tau}{g_\mu}\right) &= 1.0011 \pm 0.0015, & \left(\frac{g_\tau}{g_e}\right) &= 1.0029 \pm 0.0015, & \left(\frac{g_\mu}{g_e}\right) &= 1.0018 \pm 0.0014, \\ \left(\frac{g_\tau}{g_\mu}\right)_\pi &= 0.9963 \pm 0.0027, & \left(\frac{g_\tau}{g_\mu}\right)_K &= 0.9858 \pm 0.0071. \end{aligned} \quad (6.8)$$

Here the first three ratios are defined as

$$\left(\frac{g_\tau}{g_\mu}\right)^2 \equiv \bar{\Gamma}(\tau \rightarrow e\nu\bar{\nu})/\bar{\Gamma}(\mu \rightarrow e\nu\bar{\nu}), \quad (6.9)$$

$$\left(\frac{g_\tau}{g_e}\right)^2 \equiv \bar{\Gamma}(\tau \rightarrow \mu\nu\bar{\nu})/\bar{\Gamma}(\mu \rightarrow e\nu\bar{\nu}), \quad (6.10)$$

$$\left(\frac{g_\mu}{g_e}\right)^2 \equiv \bar{\Gamma}(\tau \rightarrow \mu\nu\bar{\nu})/\bar{\Gamma}(\tau \rightarrow e\nu\bar{\nu}). \quad (6.11)$$

and the last two ratios are from semi-hadronic processes $\tau \rightarrow \pi/K\nu$ and $\pi/K \rightarrow \mu\nu$. $\bar{\Gamma}$ denotes the partial width normalized to its SM value. The correlation matrix for the above five observables is

$$\begin{pmatrix} 1 & +0.53 & -0.49 & +0.24 & +0.12 \\ +0.53 & 1 & +0.48 & +0.26 & +0.10 \\ -0.49 & +0.48 & 1 & +0.02 & -0.02 \\ +0.24 & +0.26 & +0.02 & 1 & +0.05 \\ +0.12 & +0.10 & -0.02 & +0.05 & 1 \end{pmatrix}. \quad (6.12)$$

The theoretical values of the ratios in the L2HDM are given as

$$\begin{aligned} \left(\frac{g_\tau}{g_\mu}\right) &\approx 1 + \delta_{\text{loop}}, & \left(\frac{g_\tau}{g_e}\right) &\approx 1 + \delta_{\text{tree}} + \delta_{\text{loop}}, & \left(\frac{g_\mu}{g_e}\right) &\approx 1 + \delta_{\text{tree}}, \\ \left(\frac{g_\tau}{g_\mu}\right)_\pi &\approx 1 + \delta_{\text{loop}}, & \left(\frac{g_\tau}{g_\mu}\right)_K &\approx 1 + \delta_{\text{loop}}. \end{aligned} \quad (6.13)$$

Here δ_{tree} and δ_{loop} are respectively corrections from the tree-level diagrams mediated by H^\pm and the one-loop diagrams involved H , A and H^\pm [20, 23],

$$\delta_{\text{tree}} = \frac{m_\tau^2 m_\mu^2 t_\beta^4}{8m_{H^\pm}^4} - \frac{m_\mu^2 t_\beta^2 g(m_\mu^2/m_\tau^2)}{m_{H^\pm}^2 f(m_\mu^2/m_\tau^2)}, \quad (6.14)$$

$$\delta_{\text{loop}} = \frac{1}{16\pi^2} \frac{m_\tau^2 t_\beta^2}{v^2} \left[1 + \frac{1}{4} (H(x_A) + s_{\beta-\alpha}^2 H(x_H) + c_{\beta-\alpha}^2 H(x_h)) \right], \quad (6.15)$$

where $f(x) \equiv 1 - 8x + 8x^3 - x^4 - 12x^2 \ln(x)$, $g(x) \equiv 1 + 9x - 9x^2 - x^3 + 6x(1+x) \ln(x)$ and $H(x_\phi) \equiv \ln(x_\phi)(1+x_\phi)/(1-x_\phi)$ with $x_\phi = m_\phi^2/m_{H^\pm}^2$.

The experimental value of $\left(\frac{g_\tau}{g_e}\right)$ has an approximately 2σ positive deviation from the SM. In the L2HDM, the tree-level diagram mediated by H^\pm gives negative contribution to the decay $\tau \rightarrow \mu\nu\bar{\nu}$, as shown in Eq. (6.14), which tends to raise the discrepancy in the LFU in τ decays. In [27], a global fit to the LFU data from τ decays and the 125 GeV Higgs signal data was performed, requiring $\chi^2 - \chi_{\min}^2 \leq 6.18$ with χ_{\min}^2 denoting the minimum of χ^2 . Fig. 6 shows the surviving samples satisfying the constraints of "pre-muon $g-2$ " (denoting the theory, the oblique parameters, the exclusion limits from the searches for Higgs at LEP, the signal data of the 125 GeV Higgs, LFU in τ decays, and the exclusion limits from $h \rightarrow AA$ channels at LHC). The LFU in Z decays can exclude most of samples in the region of large m_{H^\pm} (m_H) and $\tan\beta$. In addition to a large $\tan\beta$, one-loop diagrams can give a sizable correction to the LFU in Z decays for $m_A < m_{H^\pm}$ (m_H). The oblique parameters favor H and H^\pm to have a small splitting mass for a light A . Many samples in the regions of m_A around 10 GeV and $m_{H^\pm} < 300$ GeV are excluded by the measurement of $\text{Br}(B_s \rightarrow \mu^+\mu^-)$. This is because that the decay $B_s \rightarrow \mu^+\mu^-$ can get sizable corrections from the A -exchange diagrams for a very small m_A .

Under various theoretical and experimental constraints, the L2HDM can explain the muon $g-2$ anomaly in the regions of $32 < \tan\beta < 80$, $10 \text{ GeV} < m_A < 65 \text{ GeV}$, $260 \text{ GeV} < m_H < 620 \text{ GeV}$, and $180 \text{ GeV} < m_{H^\pm} < 620 \text{ GeV}$. Because the contributions of A and H to the muon $g-2$ anomaly are respectively positive and negative, the mass splitting between A and H is required to be large to explain the muon $g-2$ anomaly, as shown in the lower-middle panel of Fig. 6.

The muon $g-2$ explanation requires a large $\tan\beta$ which will sizably suppress the quark Yukawa couplings of H , A and H^\pm . Therefore, these extra Higgs bosons are dominantly produced at the LHC via the following electroweak processes:

$$pp \rightarrow W^{\pm*} \rightarrow H^\pm A, \quad (6.16)$$

$$pp \rightarrow Z^*/\gamma^* \rightarrow HA, \quad (6.17)$$

$$pp \rightarrow W^{\pm*} \rightarrow H^\pm H, \quad (6.18)$$

$$pp \rightarrow Z^*/\gamma^* \rightarrow H^+ H^-. \quad (6.19)$$

The main decay modes of the Higgs bosons are

$$A \rightarrow \tau^+\tau^-, \mu^+\mu^-, \dots, \quad (6.20)$$

$$H \rightarrow \tau^+\tau^-, ZA, \dots, \quad (6.21)$$

$$H^\pm \rightarrow \tau^\pm\nu, W^\pm A, \dots. \quad (6.22)$$

Therefore, in the parameter space favored by the muon $g-2$ explanation, the L2HDM will mainly produce multi-lepton signature at the LHC, especially the multi- τ signature.

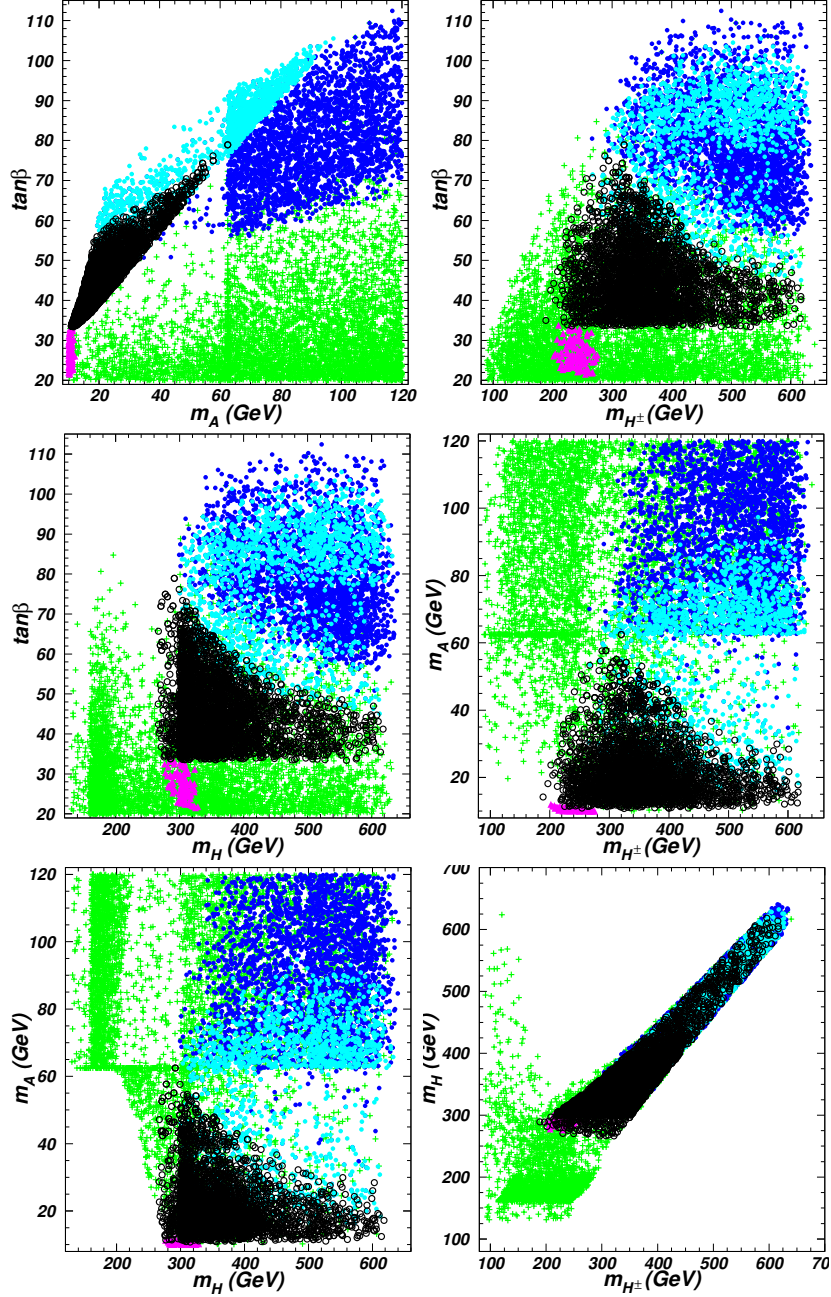


Figure 6. All the samples are allowed by the constraints of "pre-muon $g - 2$ ", taken from [27]. The triangles (pink) are excluded by the $\text{Br}(B_s \rightarrow \mu^+\mu^-)$ data, the light bullets (sky blue) and dark bullets (royal blue) are excluded by LFU in Z decay. The light (dark) bullets can (cannot) explain the muon $g - 2$ anomaly. The circles (black) are allowed by the constraints from the muon $g - 2$, "pre-muon $g - 2$ ", the LFU in Z decay, and $\text{Br}(B_s \rightarrow \mu^+\mu^-)$.

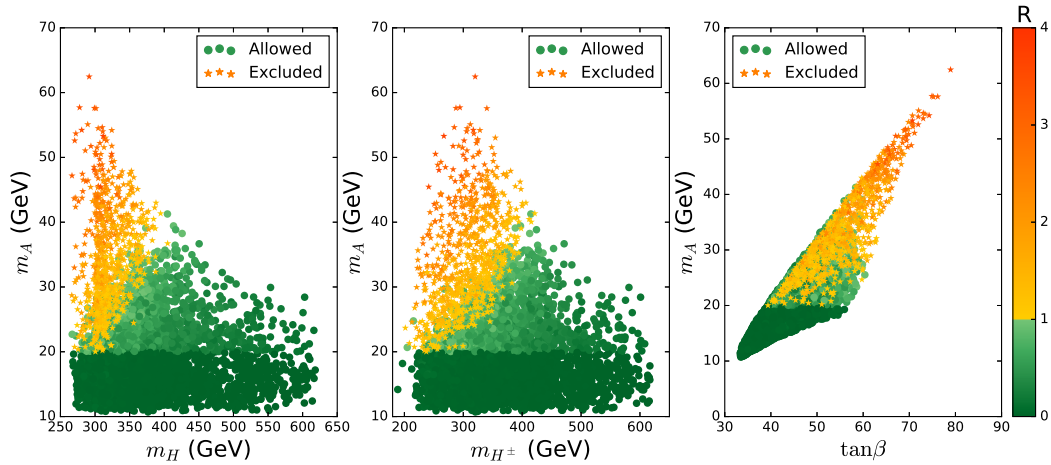


Figure 7. All the samples are allowed by the constraints from the muon $g-2$, "pre-muon $g-2$ ", the LFU in Z decay, and $\text{Br}(B_s \rightarrow \mu^+ \mu^-)$, taken from [27]. The orange stars and green dots are excluded and allowed by the LHC Run-2 data at 95% confidence level, respectively.

The study in [27] used all the analysis for the 13 TeV LHC in CheckMATE 2.0.7 [181] and the multi-lepton searches for electroweakino [182–186] to constrain the parameter space. The surviving samples are shown in Fig. 7 in which $R > 1$ denotes that the corresponding samples are excluded at 95% confidence level. The searches for multi-leptons at the 13 TeV LHC shrink m_A from [10, 65] GeV to [10, 44] GeV and $\tan\beta$ from [32, 80] to [32, 60]. The main constraint is given by the search for electroweak production of charginos and neutralinos in multi-lepton final states [183].

For relatively large m_H and m_{H^\pm} , the production cross sections of extra Higgs bosons are small enough to escape the limits of direct searches at the LHC. For a light A , the τ leptons from the decays of A produced in Eq. (6.16) and Eq. (6.17) are too soft to be distinguished at detectors, and the τ leptons from A produced in H/H^\pm decays are collinear because of the large mass splitting between A and H/H^\pm . Thus, in the very low m_A region, the acceptance of above signal region quickly decreases and the limits of direct searches can be easily satisfied.

6.2 Solution of muon $g-2$ and τ decays

The L2HDM can give a simple explanation for the muon $g-2$, but raise the discrepancy in the LFU in τ decays. Therefore, to explain the muon $g-2$ and LFU of τ decays simultaneously, other models need to be considered.

6.2.1 Lepton specific inert 2HDM

In this model the Z_2 symmetry-breaking lepton Yukawa interactions of Φ_2 are added to the inert 2HDM [187, 188]

$$-\mathcal{L} = \frac{\sqrt{2}m_e}{v} \kappa_e \bar{L}_{1L} \Phi_2 e_R + \frac{\sqrt{2}m_\mu}{v} \kappa_\mu \bar{L}_{2L} \Phi_2 \mu_R + \frac{\sqrt{2}m_\tau}{v} \kappa_\tau \bar{L}_{3L} \Phi_2 \tau_R + \text{h.c.} . \quad (6.23)$$

In this way the extra Higgs bosons (H , A , and H^\pm) acquire couplings to the leptons while have no couplings to the quarks.

In this model, $\left(\frac{g_\tau}{g_e}\right)^2$ is given by

$$\left(\frac{g_\tau}{g_e}\right)^2 \approx \frac{1 + 2\delta_{\text{tree}} + 2\delta_{\text{loop}}^\tau}{1 + 2\delta_{\text{loop}}^\mu}. \quad (6.24)$$

Here δ_{tree} and $\delta_{\text{loop}}^{\tau,\mu}$ are respectively corrections from the tree-level diagrams mediated by H^\pm and the one-loop diagrams involving H , A and H^\pm , given by [20, 23, 27]

$$\delta_{\text{tree}} = \frac{m_\tau^2 m_\mu^2}{8m_{H^\pm}^4} \kappa_\tau^2 \kappa_\mu^2 - \frac{m_\mu^2}{m_{H^\pm}^2} \kappa_\tau \kappa_\mu \frac{g(m_\mu^2/m_\tau^2)}{f(m_\mu^2/m_\tau^2)}, \quad (6.25)$$

$$\delta_{\text{loop}}^{\tau,\mu} = \frac{1}{16\pi^2} \frac{m_{\tau,\mu}^2}{v^2} \kappa_{\tau,\mu}^2 \left[1 + \frac{1}{4} (H(x_A) + H(x_H)) \right]. \quad (6.26)$$

The model gives the one-loop contributions to muon $g-2$ [172–174]

$$\Delta a_\mu^{\text{2HDM}}(\text{1loop}) = \frac{m_\mu^2}{8\pi^2 v^2} \sum_i \kappa_\mu^2 r_\mu^i F_j(r_\mu^i), \quad (6.27)$$

where $i = H, A, H^\pm$ and $r_\mu^i = m_\mu^2/M_j^2$.

The contributions of the two-loop diagrams are

$$\Delta a_\mu^{\text{2HDM}}(\text{2loop}) = \frac{m_\mu^2}{8\pi^2 v^2} \frac{\alpha_{\text{em}}}{\pi} \sum_{i,\ell} Q_\ell^2 \kappa_\mu \kappa_\ell r_\ell^i G_i(r_\ell^i), \quad (6.28)$$

where $i = H, A$, $\ell = \tau$, and m_ℓ and Q_ℓ are the mass and electric charge of the lepton ℓ in the loop.

This model was also used to discuss the electron $g-2$ anomaly, and the calculations are similar to the muon $g-2$. The value from the measurement of the fine-structure constant using ^{133}Cs atoms at Berkeley [189] makes the electron $g-2$ to have 2.4σ deviation from the SM prediction [190, 191],

$$\Delta a_e = a_e^{\text{exp}} - a_e^{\text{SM}} = (-87 \pm 36) \times 10^{-14}. \quad (6.29)$$

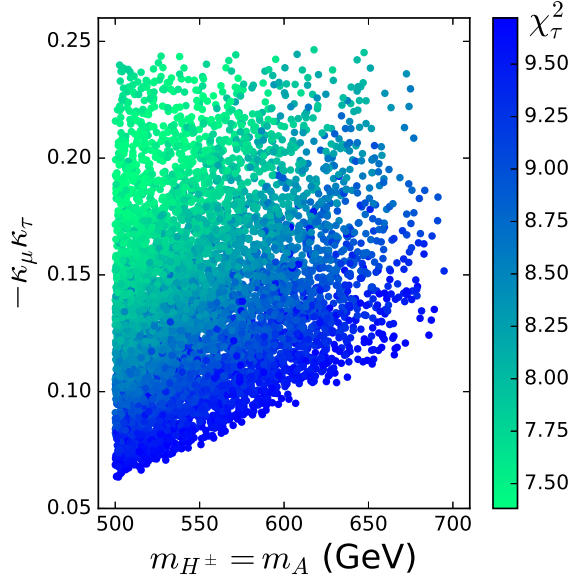


Figure 8. In the lepton-specific inert 2HDM, the surviving samples fit the data of LFU in τ decay within the 2σ range, taken from [187].

However, the newest experimental result of the fine-structure constant using ^{87}Rb atoms at Laboratoire Kastler Brossel gives a value of a_e which agrees well with the SM value [192]. So far, the discrepancy between these two experimental results is not clear. If the Berkeley ^{133}Cs experiment result turns out to be the real story, it will be challenging to explain muon and electron $g - 2$ simultaneously since the two effects have opposite sign. In [187], the Berkeley ^{133}Cs experiment data was used and this model was found to give explanation for the muon and electron $g - 2$ (for the explanation in other popular models like the minimal supersymmetry, see, e.g., [193]).

Taking

$$\kappa_\mu < 0, \quad \kappa_\tau > 0, \quad \kappa_e > 0, \quad (6.30)$$

then δ_{tree} has a positive value because of the opposite signs of κ_μ and κ_τ . Thus, the model can enhance $\left(\frac{g_\tau}{g_e}\right)$ and give a better fit to the data of the LFU in the τ decays. The contributions of H (A) to the muon $g - 2$ are positive (negative) at the two-loop level and positive (negative) at one-loop level. For the electron $g - 2$, the contributions of H (A) are negative (positive) at the two-loop level and positive (negative) at one-loop level. Fig. 8 shows the surviving samples with $\chi_\tau^2 < 9.72$, which means to fit the data of LFU in τ decays within 2σ range. Fig. 8 shows that χ_τ^2 can be as low as 7.4, which is much smaller than the SM prediction (12.25). Fig. 9 shows that after imposing the constraints of theory, the oblique parameters, the Z decay, and the direct searches at LHC, the model can simultaneously explain the anomalies of Δa_μ , Δa_e and LFU in the τ decay within 2σ range in a large parameter space of $200 \text{ GeV} < m_H < 320 \text{ GeV}$, $500 \text{ GeV} < m_A = m_{H^\pm} < 680 \text{ GeV}$, $0.0066 < \kappa_e < 0.01$, $-0.25 < \kappa_\mu < -0.147$, and $0.53 < \kappa_\tau < 1.0$.

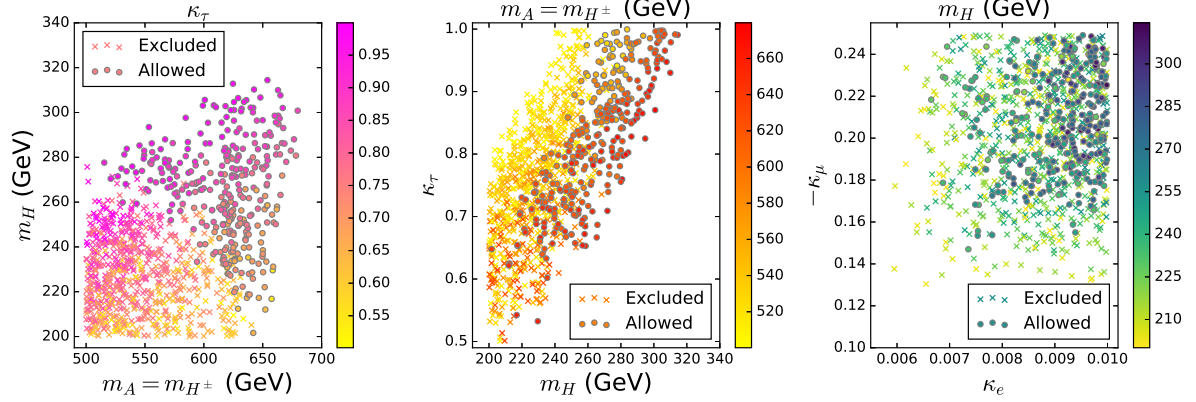


Figure 9. All the samples are allowed by the constraints of theory, the oblique parameters, Δa_μ , Δa_e , the data of LFU in τ decays, and Z decay, taken from [187]. The bullets and crosses are respectively allowed and excluded by the direct search limits from the LHC at 95% confidence level. The colors denote κ_τ , m_A and m_H in left, middle, and right panel, respectively.

Table 4. The Z_4 charge assignment of μ - τ -philic 2HDM.

	Φ_1	Φ_2	Q_L^i	U_R^i	D_R^i	L_L^e	L_L^μ	L_L^τ	e_R	μ_R	τ_R
Z_4	1	-1	1	1	1	1	i	-i	1	i	-i

6.2.2 μ - τ -philic Higgs doublet model

In this model an exact discrete Z_4 symmetry is imposed, and the Z_4 charge assignment is shown in Table 4 [194]. The scalar potential is given as

$$\begin{aligned}
V = & Y_1(\Phi_1^\dagger \Phi_1) + Y_2(\Phi_2^\dagger \Phi_2) + \frac{\lambda_1}{2}(\Phi_1^\dagger \Phi_1)^2 + \frac{\lambda_2}{2}(\Phi_2^\dagger \Phi_2)^2 \\
& + \lambda_3(\Phi_1^\dagger \Phi_1)(\Phi_2^\dagger \Phi_2) + \lambda_4(\Phi_1^\dagger \Phi_2)(\Phi_2^\dagger \Phi_1) + \left[\frac{\lambda_5}{2}(\Phi_1^\dagger \Phi_2)^2 + \text{h.c.} \right]. \quad (6.31)
\end{aligned}$$

The vev of the Φ_1 field is $v=246$ GeV, while the Φ_2 field has zero VEV. The fermions obtain masses via the Yukawa interactions with Φ_1

$$-\mathcal{L} = y_u \bar{Q}_L \tilde{\phi}_1 U_R + y_d \bar{Q}_L \phi_1 D_R + y_\ell \bar{L}_L \phi_1 E_R + \text{h.c.} \quad (6.32)$$

The Z_4 symmetry allows Φ_2 to have μ - τ interactions [194]

$$-\mathcal{L}_{\text{LFV}} = \sqrt{2} \rho_{\mu\tau} \bar{L}_L^\mu \phi_2 \tau_R + \sqrt{2} \rho_{\tau\mu} \bar{L}_L^\tau \phi_2 \mu_R + \text{h.c.} \quad (6.33)$$

From these interactions we can obtain the μ - τ lepton flavor violation (LFV) couplings of H , A , and H^\pm .

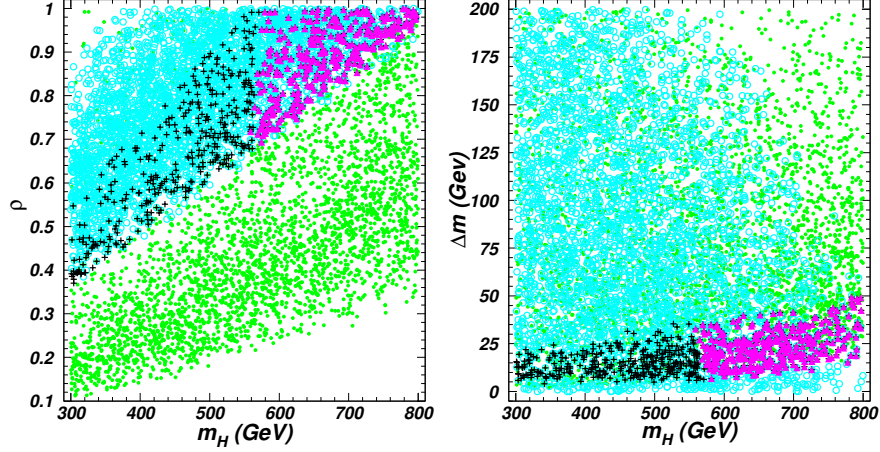


Figure 10. The surviving samples of the μ - τ -philic 2HDM allowed by the constraints of the theory, the oblique parameters, and the Z decays, taken from [198]. The bullets (green) samples are within the 2σ range of muon $g-2$ and the circles (blue) are within the 2σ range of LFU in the τ decays. The triangles (purple) and pluses (black) are within the 2σ ranges of both muon $g-2$ and LFU in the τ decays, and the former are allowed by the limits of the direct searches at the LHC, while the latter are excluded. Here $\Delta m \equiv m_A - m_H$ with $m_A = m_{H^\pm}$.

The model gives new contribution to Δa_μ via the one-loop diagrams containing the μ - τ LFV coupling of H and A [195–197]

$$\Delta a_\mu = \frac{m_\mu m_\tau \rho^2}{8\pi^2} \left[\frac{(\log \frac{m_H^2}{m_\tau^2} - \frac{3}{2})}{m_H^2} - \frac{\log(\frac{m_A^2}{m_\tau^2} - \frac{3}{2})}{m_A^2} \right], \quad (6.34)$$

which shows that the contributions of H and A are respectively positive and negative.

In this model, $(\frac{g_\tau}{g_e})^2$ is given as [194, 198]

$$\left(\frac{g_\tau}{g_e}\right)^2 = (1 + \delta_{\text{loop}}^\tau)^2 + \frac{\delta_{\text{tree}}}{(1 + \delta_{\text{loop}}^\mu)^2}, \quad (6.35)$$

where the flavor of final neutrino and anti-neutrino states is summed up, and δ_{tree} is from the tree-level diagram mediated by the charged Higgs

$$\delta_{\text{tree}} = 4 \frac{m_W^4 \rho^4}{g^4 m_{H^\pm}^4}, \quad (6.36)$$

with $\rho_{\mu\tau} = \rho_{\tau\mu} = \rho$, and δ_{loop}^μ and $\delta_{\text{loop}}^\tau$ are the corrections to vertices $W\bar{\nu}_\mu\mu$ and $W\bar{\nu}_\tau\tau$ from the one-loop diagrams involving A , H , and H^\pm

$$\delta_{\text{loop}}^\tau = \delta_{\text{loop}}^\mu = \frac{1}{16\pi^2} \rho^2 \left[1 + \frac{1}{4} (H(x_A) + H(x_H)) \right]. \quad (6.37)$$

Since δ_{tree} is positive, the model can enhance $(\frac{g_\tau}{g_e})$ and give a better fit to the data of the LFU in the τ decays.

Fig. 10 shows that after considering the constraints from theory, the oblique parameters and the Z decay, the model can simultaneously explain Δa_μ and LFU in the τ decays in the parameter space with $300 \text{ GeV} < m_H < 800 \text{ GeV}$ and $\Delta m < 50 \text{ GeV}$. For such small mass splitting between m_A (m_{H^\pm}) and m_H , H , A and H^\pm will mainly decay into $\tau\mu$, $\tau\nu_\mu$, and $\mu\nu_\tau$. The limits of direct searches at the LHC exclude the region $m_H < 560 \text{ GeV}$ and require $\rho > 0.68$. Also Refs. [199, 200] discussed the implications of the muon $g-2$ anomaly on the model.

In the discussions above, m_A and m_{H^\pm} are chosen to have degenerate mass, which is disfavored by the CDF W -mass. The study in Ref. [59] found that combined with relevant theoretical and experimental constraints, the mass splittings among H , A and H^\pm of the model are stringently constrained in the region simultaneously explaining the W -mass, muon $g-2$ and LFU in τ decays, i.e., $10 \text{ GeV} < m_A - m_H < 75 \text{ GeV}$, $65 \text{ GeV} < m_{H^\pm} - m_A < 100 \text{ GeV}$, $85 \text{ GeV} < m_{H^\pm} - m_H < 125 \text{ GeV}$ ($-150 \text{ GeV} < m_{H^\pm} - m_A < -85 \text{ GeV}$, $-105 \text{ GeV} < m_{H^\pm} - m_H < -55 \text{ GeV}$).

6.3 Other 2HDMs and muon $g-2$

In [201] the authors proposed a muon specific 2HDM in which extra Higgs boson couplings to muon are enhanced by a factor of $\tan\beta$, while their couplings to the other fermions are suppressed by $\cot\beta$. Thus, the model can explain the muon $g-2$ anomaly by the contributions of the one-loop diagram for a very large $\tan\beta$, and weaken the constraints of the τ decays because of the cancellation of $\tan\beta$ between the tau and the muon Yukawa couplings to the charged Higgs. The study in [24] considered a perturbed lepton-specific 2HDM in which the sign of extra Higgs boson couplings to tau are flipped. Similar to the lepton-specific inert 2HDM, the model can accommodate the muon $g-2$ anomaly and the τ decays, but the electron $g-2$ anomaly is not simultaneously explained. The muon and electron $g-2$ anomalies can be both explained in general 2HDM. For recent studies see e.g. [202–204].

The L2HDM can be derived from the aligned 2HDM by taking the specific parameter space [14]. Therefore, the aligned 2HDM may explain the muon $g-2$ anomaly in a broader parameter space, and the large lepton Yukawa couplings of A still play the main role in most of parameter space [205]. Some recent studies have been done in [206–210]. In addition to the 2HDM with a Z_4 symmetry, the extra Higgs doublet with the μ - τ LFV interactions can be obtained in general 2HDM. For recent studies see e.g. [211–217].

7 Summary

From the above review we summarize the following points for the 2HDMs: (i) For the popular type-II 2HDM, the current direct searches at the LHC excluded a large part of parameter space, while still allowing the 125 GeV Higgs to have wrong-sign Yukawa couplings to the down-type quarks and leptons. If a real singlet scalar DM is added to the type-II 2HDM and the 125 GeV Higgs with wrong-sign Yukawa couplings is taken as the portal between the SM sector and DM, this model can have isospin-violating interactions between DM and nucleons,

which can relax the constraints from the DM direct detections; (ii) As a simpler DM model, in several DM mass ranges the inert 2HDM can produce the correct relic density and satisfy the bounds of DM direct detections and direct searches at the LHC; (iii) The muon $g - 2$ anomaly can be explained in the lepton-specific 2HDM with a light A and heavy H/H^\pm , but it will raise the discrepancy in the LFU in τ decays. Such a tension may be solved in the 2HDM with some specific muon and tau Yukawa couplings. So, compared with low energy supersymmetry (for recent reviews see, e.g., [218, 219]), the 2HDMs can also do the job of explaining dark matter and muon $g - 2$, albeit cannot address the naturalness problem.

Acknowledgments

This work was supported by the National Natural Science Foundation of China (NNSFC) under grant Nos. 11975013, 11821505, 12075300 and 12105248, by Peng-Huan-Wu Theoretical Physics Innovation Center (12047503), by the CAS Center for Excellence in Particle Physics (CCEPP), and by the Key Research Program of the Chinese Academy of Sciences, Grant NO. XDPB15.

References

- [1] T. D. Lee, A Theory of Spontaneous Violation, *Phys. Rev. D* **8**, (1973) 1226.
- [2] H. E. Haber, G. L. Kane and T. Sterling, The Fermion Mass Scale and Possible Effects of Higgs Bosons on Experimental Observables, *Nucl. Phys. B* **161**, 493 (1979).
- [3] L. J. Hall and M. B. Wise, Flavor changing Higgs boson couplings, *Nucl. Phys. B* **187**, 397 (1981).
- [4] J. F. Donoghue and L. F. Li, Properties of Charged Higgs Bosons, *Phys. Rev. D* **19**, 945 (1979).
- [5] V. D. Barger, J. L. Hewett and R. J. N. Phillips, New Constraints on the Charged Higgs Sector in Two Higgs Doublet Models, *Phys. Rev. D* **41**, 3421 (1990).
- [6] Y. Grossman, Phenomenology of models with more than two Higgs doublets, *Nucl. Phys. B* **426**, 355 (1994).
- [7] A. G. Akeroyd and W. J. Stirling, Light charged Higgs scalars at high-energy e^+e^- colliders, *Nucl. Phys. B* **447**, 3 (1995).
- [8] A. G. Akeroyd, Nonminimal neutral Higgs bosons at LEP-2, *Phys. Lett. B* **377**, 95 (1996).
- [9] A. G. Akeroyd, Fermiophobic and other nonminimal neutral Higgs bosons at the LHC, *J. Phys. G* **24**, 1983 (1998).
- [10] M. Aoki, S. Kanemura, K. Tsumura and K. Yagyu, Models of Yukawa interaction in the two Higgs doublet model, and their collider phenomenology, *Phys. Rev. D* **80**, 015017 (2009).
- [11] N. G. Deshpande, E. Ma, Pattern of Symmetry Breaking with Two Higgs Doublets, *Phys. Rev. D* **18**, 2574 (1978).
- [12] R. Barbieri, L. J. Hall, V. S. Rychkov, Improved naturalness with a heavy Higgs: An Alternative road to LHC physics, *Phys. Rev. D* **74**, 015007 (2006)

- [13] L. Lopez Honorez, E. Nezri, J. F. Oliver et al., The Inert Doublet Model: An Archetype for Dark Matter, *JCAP* **02**, 028 (2007).
- [14] A. Pich, P. Tuzon, Yukawa Alignment in the Two-Higgs-Doublet Model, *Phys. Rev. D* **80**, (2009) 091702.
- [15] G. C. Branco, W. Grimus, L. Lavoura, Relating the scalar flavor changing neutral couplings to the CKM matrix, *Phys. Lett. B* **380**, (1996) 119-126.
- [16] J. Cao, P. Wan, L. Wu and J. M. Yang, Lepton-Specific Two-Higgs Doublet Model: Experimental Constraints and Implication on Higgs Phenomenology, *Phys. Rev. D* **80**, (2009) 071701.
- [17] J. S. Lee and A. Pilaftsis, Radiative Corrections to Scalar Masses and Mixing in a Scale Invariant Two Higgs Doublet Model, *Phys. Rev. D* **86**, (2012) 035004.
- [18] A. Broggio, E. J. Chun, M. Passera, K. M. Patel and S. K. Vempati, Limiting two-Higgs-doublet models, *JHEP* **1411**, (2014) 058.
- [19] L. Wang and X. F. Han, A light pseudoscalar of 2HDM confronted with muon $g-2$ and experimental constraints, *JHEP* **05**, (2015) 039.
- [20] T. Abe, R. Sato and K. Yagyu, Lepton-specific two Higgs doublet model as a solution of muon $g - 2$ anomaly, *JHEP* **1507**, (2015) 064.
- [21] E. J. Chun, Z. Kang, M. Takeuchi, Y.-L. Tsai, LHC τ -rich tests of lepton-specific 2HDM for $(g - 2)_\mu$, *JHEP* **1511**, (2015) 099.
- [22] X. Liu, L. Bian, X.-Q. Li, J. Shu, Type-III two Higgs doublet model plus a pseudoscalar confronted with $h \rightarrow \mu\tau$, muon $g - 2$ and dark matter, *Nucl. Phys. B* **909**, (2016) 507-524.
- [23] E. J. Chun, J. Kim, Leptonic Precision Test of Leptophilic Two-Higgs-Doublet Model, *JHEP* **1607**, (2016) 110.
- [24] A. Crivellin, J. Heeck, P. Stoffer, Perturbed Lepton-Specific Two-Higgs-Doublet Model Facing Experimental Hints for Physics beyond the Standard Model, *Phys. Rev. Lett.* **116**, (2016) 081801.
- [25] B. Batell, N. Lange, D. McKeen, M. Pospelov, A. Ritz, Muon anomalous magnetic moment through the leptonic Higgs portal, *Phys. Rev. D* **95**, (2017) 075003.
- [26] L. Wang, J. M. Yang, Y. Zhang, Probing a pseudoscalar at the LHC in light of $R(D^{(*)})$ and muon $g - 2$ excesses, *Nucl. Phys. B* **924**, (2017) 47-62.
- [27] L. Wang, J. M. Yang, M. Zhang, Y. Zhang, Revisiting lepton-specific 2HDM in light of muon $g - 2$ anomaly, *Phys. Lett. B* **788**, (2019) 519-529.
- [28] A. Jueid, J. Kim, S. Lee, J. Song, Type-X two-Higgs-doublet model in light of the muon $g - 2$: Confronting Higgs boson and collider data, *Phys. Rev. D* **104**, (2021) 095008.
- [29] A. Cherchiglia, P. Kneschke, D. Stockinger, H. Stöckinger-Kim, The muon magnetic moment in the 2HDM: complete two-loop result, *JHEP* **1701**, (2017) 007.
- [30] A. Cherchiglia, D. Stöckinger, H. Stöckinger-Kim, Muon $g - 2$ in the 2HDM: maximum results and detailed phenomenology, *Phys. Rev. D* **98**, (2018) 035001.

- [31] D. Sabatta, A. S. Cornell, A. Goyal, M. Kumar, B. Mellado, Connecting muon anomalous magnetic moment and multi-lepton anomalies at LHC, *Chin. Phys. C* **44**, (2020) 063103.
- [32] E. J. Chun, S. Dwivedi, T. Mondal, B. Mukhopadhyaya, S. K. Rai, Reconstructing heavy Higgs boson masses in a type X two-Higgs-doublet model with a light pseudoscalar particle, *Phys. Rev. D* **98**, (2018) 075008.
- [33] A. Dey, J. Lahiri, B. Mukhopadhyaya, Muon $g - 2$ and a type-X two Higgs doublet scenario: some studies in high-scale validity, arXiv:2106.01449.
- [34] X.-G. He, T. Li, X.-Q. Li, J. Tandean, H.-C. Tsai, Constraints on Scalar Dark Matter from Direct Experimental Searches, *Phys. Rev. D* **79**, 023521 (2009).
- [35] X.-G. He, J. Tandean, Low-Mass Dark-Matter Hint from CDMS II, Higgs Boson at the LHC, and Darkon Models, *Phys. Rev. D* **88**, 013020 (2013).
- [36] Y. Cai, T. Li, Singlet dark matter in a type II two Higgs doublet model, *Phys. Rev. D* **88**, 115004 (2013).
- [37] L. Wang, X.-F. Han, A simplified 2HDM with a scalar dark matter and the galactic center gamma-ray excess, *Phys. Lett. B* **739**, 416-420 (2014).
- [38] A. Drozd, B. Grzadkowski, J. F. Gunion, Y. Jiang, Extending two-Higgs-doublet models by a singlet scalar field - the Case for Dark Matter, *JHEP* **1411**, 105 (2014).
- [39] A. Drozd, B. Grzadkowski, J. F. Gunion, Y. Jiang, Isospin-violating dark-matter-nucleon scattering via two-Higgs-doublet-model portals, *JCAP* **1610**, 040 (2016).
- [40] X.-G. He, J. Tandean, New LUX and PandaX-II Results Illuminating the Simplest Higgs-Portal Dark Matter Models, *JHEP* **1612**, 074 (2016).
- [41] T. Alanne, K. Kainulainen, K. Tuominen, V. Vaskonen, Baryogenesis in the two doublet and inert singlet extension of the Standard Model, *JCAP* **1608**, 057 (2016).
- [42] L. Wang, R. Shi, X.-F. Han, Wrong sign Yukawa coupling of the 2HDM with a singlet scalar as dark matter confronted with dark matter and Higgs data, *Phys. Rev. D* **96**, 115025 (2017).
- [43] N. Chen, Z. Kang, J. Li, Missing particle associated with two bottom quarks at the LHC: Mono-bb versus 2bb with razor variables, *Phys. Rev. D* **95**, 015003 (2017).
- [44] L. Wang, R. Shi, X.-F. Han, B. Zhu, Light scalar dark matter extension of the type-II two-Higgs-doublet model, *Phys. Rev. D* **98**, (2018) 035024.
- [45] S. Baum, N. R. Shah, Two Higgs Doublets and a Complex Singlet: Disentangling the Decay Topologies and Associated Phenomenology, *JHEP* **12**, (2018) 044.
- [46] Z. Zhang, C. Cai, X.-M. Jiang, Y.-L. Tang, Z.-H. Yu, Phase transition gravitational waves from pseudo-Nambu-Goldstone dark matter and two Higgs doublets, *JHEP* **05**, (2021) 160.
- [47] W. Altmannshofer, B. Maddock, S. Profumo, Doubly Blind Spots in Scalar Dark Matter Models, *Phys. Rev. D* **100**, (2019) 055033.
- [48] M. E. Cabrera, J. A. Casas, A. Delgado, S. Robles, Generalized Blind Spots for Dark Matter Direct Detection in the 2HDM, *JHEP* **02**, (2020) 166.
- [49] P. Bandyopadhyay, E. J. Chun, R. Mandal, Scalar Dark Matter in Leptophilic Two-Higgs-Doublet Model, *Phys. Lett. B* **779**, (2018) 201-205.

- [50] A. Dey, J. Lahiri, Collider Signatures of Type-X 2HDM + scalar singlet dark matter at HL-LHC, arXiv:2112.15536.
- [51] CMS Collaboration, S. Chatrchyan et al., Observation of a new boson at a mass of 125 GeV with the CMS experiment at the LHC, Phys. Lett. B **716**, 30 (2012).
- [52] ATLAS Collaboration, G. Aad et al., Observation of a new particle in the search for the Standard Model Higgs boson with the ATLAS detector at the LHC, Phys. Lett. B **716**, 1 (2012).
- [53] CMS Collaboration, A. M. Sirunyan et al., Search for a standard model-like Higgs boson in the mass range between 70 and 110 GeV in the diphoton final state in proton-proton collisions at $\sqrt{s} = 8$ and 13 TeV, Phys. Lett. B **793**, (2019) 320-347.
- [54] ATLAS Collaboration, Search for a light charged Higgs boson in $t \rightarrow H^+ b$ decays, with $H^+ \rightarrow cb$, in the lepton+jets final state in proton-proton collisions at $\sqrt{s} = 13$ TeV with the ATLAS detector, ATLAS-CONF-2021-037.
- [55] CDF Collaboration, High-precision measurement of the W boson mass with the CDF II detector, Science **376**, 6589 (2022) 170.
- [56] Y.-Z. Fan, T.-P. Tang, Y.-L. S. Tsai, L. Wu, Inert Higgs Dark Matter for New CDF W-boson Mass and Detection Prospects, arXiv:2204.03693.
- [57] H. Song, W. Su, M. Zhang, Electroweak Phase Transition in 2HDM under Higgs, Z-pole, and W precision measurements, arXiv:2204.05085.
- [58] K. S. Babu, S. Jana, P. K. Vishnu, Correlating W-Boson Mass Shift with Muon $g - 2$ in the 2HDM, arXiv:2204.05303.
- [59] X.-F. Han, F. Wang, L. Wang, J. Yang, Y. Zhang, A joint explanation of W-mass and muon $g - 2$ in 2HDM, arXiv:2204.06505.
- [60] S. Lee, K. Cheung, J. Kim, C.-T. Lu, J. Song, Status of the two-Higgs-doublet model in light of the CDF m_W measurement, arXiv:2204.10338.
- [61] R. Benbrik, M. Boukidi, B. Manaut, W-mass and 96 GeV excess in type-III 2HDM, arXiv:2204.11755.
- [62] H. Abouabid, A. Arhrib, R. Benbrik, M. Krab, M. Ouchemhou, Is the new CDF M_W measurement consistent with the two Higgs doublet model?, arXiv:2204.12018.
- [63] K. Ghorbani, P. Ghorbani, W-Boson Mass Anomaly from Scale Invariant 2HDM, arXiv:2204.09001.
- [64] G. Arcadi, A. Djouadi, The 2HD+a model for a combined explanation of the possible excesses in the CDF M_W measurement and $(g - 2)_\mu$ with Dark Matter, arXiv:2204.08406.
- [65] R. Benbrik, M. Boukidi, S. Moretti, S. Semlali, Explaining the 96 GeV Di-photon Anomaly in a Generic 2HDM Type-III, arXiv:2204.07470.
- [66] T. Biekötter, S. Heinemeyer, G. Weiglein, Excesses in the low-mass Higgs-boson search and the WW-boson mass measurement, arXiv:2204.05975.
- [67] H. Bahl, J. Braathen, G. Weiglein, New physics effects on the WW-boson mass from a doublet extension of the SM Higgs sector, arXiv:2204.05269

- [68] F. J. Botella, F. Cornet-Gomez, C. Miro, M. Nebot, Muon and electron $g - 2$ anomalies in a flavor conserving 2HDM with an oblique view on the CDF M_W value, arXiv:2205.01115.
- [69] J. Kim, Compatibility of muon $g - 2$, WW mass anomaly in type-X 2HDM, arXiv:2205.01437
- [70] G. C. Branco, P. M. Ferreira, L. Lavoura, M. N. Rebelo, M. Sher, Theory and phenomenology of two-Higgs-doublet models, Phys. Rept. **516** (2012) 1-102.
- [71] G. Bhattacharyya, D. Das, Scalar sector of two-Higgs-doublet models: A minireview, Pramana **87**, (2016) 40.
- [72] R. Aggleton, D. Barducci, N.-E. Bomark, S. Moretti, C. Shepherd-Themistocleous, Review of LHC experimental results on low mass bosons in multi Higgs models , JHEP **02**, (2017) 035.
- [73] H. Davoudiasl, I. M. Lewis, M. Sullivan, Good things to do with extra Higgs doublets, arXiv:2203.01396.
- [74] I. P. Ivanov, Building and testing models with extended Higgs sectors, Prog. Part. Nucl. Phys. **95**, (2017) 160-208.
- [75] T. Robens, The THDMa Revisited, Symmetry **13**, (2021) 2341.
- [76] E. Ma, Verifiable radiative seesaw mechanism of neutrino mass and dark matter, Phys. Rev. D **73**, (2006) 077301.
- [77] A. Barroso, P. M. Ferreira, I. P. Ivanov, R. Santos, Metastability bounds on the two Higgs doublet model, JHEP **06**, (2013) 045.
- [78] B. W. Lee, C. Quigg, H. B. Thacker, Weak Interactions at Very High-Energies: The Role of the Higgs Boson Mass, Phys. Rev. D **16**, (1977) 1519.
- [79] M. D. Goodsell, F. Staub, Unitarity constraints on general scalar couplings with SARAH, Eur. Phys. Jour. C **78**, (2018) 649.
- [80] S. Kanemura, T. Kubota, E. Takasugi, Lee-Quigg-Thacker bounds for Higgs boson masses in a two doublet model, Phys. Lett. B **313**, (1993) 155.
- [81] A. G. Akeroyd, A. Arhrib, E. Naimi, Note on tree-level unitarity in the general two Higgs doublet model, Phys. Lett. B **490**, (2000) 119.
- [82] M. D. Goodsell, F. Staub, Improved unitarity constraints in Two-Higgs-Doublet-Models, Phys. Lett. B **788**, (2019) 206-212.
- [83] H.-J. He, N. Polonsky, S. Su, Extra families, Higgs spectrum and oblique corrections, Phys. Rev. D **64**, (2001) 053004.
- [84] H. E. Haber, D. O'Neil, Basis-independent methods for the two-Higgs-doublet model. III. The CP-conserving limit, custodial symmetry, and the oblique parameters S, T, U, Phys. Rev. D **83**, (2011) 055017.
- [85] A. Celis, V. Ilisie, A. Pich, LHC constraints on two-Higgs doublet models, JHEP **07**, (2013) 053.
- [86] M. Tanabashi et al., Review of Particle Physics, [Particle Data Group], Phys. Rev. D **98**, 030001 (2018).
- [87] L. Wang, X.-F. Han, H.-X. Wang, Revisiting wrong sign Yukawa coupling of type II two-Higgs-doublet model in light of recent LHC data, Chin. Phys. C **44**, (2020) 073101.

- [88] M. Misiak, M. Steinhauser, Weak radiative decays of the B meson and bounds on M_{H^\pm} in the Two-Higgs-Doublet Model, *Eur. Phys. Jour. C* **77**, 201 (2017).
- [89] P. A. Zyla et al., Review of Particle Physics, *PTEP* **2020**, (2020) 083C01.
- [90] C.-T. Lu, L. Wu, Y. Wu, B. Zhu, Electroweak Precision Fit and New Physics in light of WW Boson Mass, arXiv:2204.03796.
- [91] M. E. Peskin and T. Takeuchi, Estimation of oblique electroweak corrections, *Phys. Rev. D* **46**, (1992) 381-409.
- [92] J. Bernon, J. F. Gunion, H. E. Haber, Y. Jiang, S. Kraml, Scrutinizing the alignment limit in two-Higgs-doublet model: $m_h = 125$ GeV, *Phys. Rev. D* **92**, 075004 (2015).
- [93] P. S. Bhupal Dev, A. Pilaftsis, Maximally Symmetric Two Higgs Doublet Model with Natural Standard Model Alignment, *JHEP* **12**, 024 (2014).
- [94] I. F. Ginzburg, M. Krawczyk, P. Osland, Resolving SM like scenarios via Higgs boson production at a photon collider. 1. 2HDM versus SM, arXiv:hep-ph/0101208.
- [95] P. M. Ferreira, J. F. Gunion, H. E. Haber and R. Santos, Probing wrong-sign Yukawa couplings at the LHC and a future linear collider, *Phys. Rev. D* **89**, 115003 (2014).
- [96] B. Dumont, J. F. Gunion, Y. Jiang and S. Kraml, Constraints on and future prospects for Two-Higgs-Doublet Models in light of the LHC Higgs signal, *Phys. Rev. D* **90**, 035021 (2014).
- [97] D. Fontes, J. C. Romão and J. P. Silva, A reappraisal of the wrong-sign $hb\bar{b}$ coupling and the study of $h \rightarrow Z\gamma$, *Phys. Rev. D* **90**, 015021 (2014).
- [98] L. Wang, X.-F. Han, Status of the aligned two-Higgs-doublet model confronted with the Higgs data, *JHEP* **1404**, (2014) 128.
- [99] P. M. Ferreira, J. F. Gunion, H. E. Haber, R. Santos, Probing wrong-sign Yukawa couplings at the LHC and a future linear collider, *Phys. Rev. D* **89**, 115003 (2014).
- [100] P. M. Ferreira, R. Guedes, M. O. P. Sampaio, R. Santos, Wrong sign and symmetric limits and non-decoupling in 2HDMs, *JHEP* **1412**, 067 (2014).
- [101] L. Wang, X.-F. Han, A light pseudoscalar of 2HDM confronted with muon $g - 2$ and experimental constraints, *JHEP* **1505**, 039 (2015).
Study of the heavy CP-even Higgs with mass 125 GeV in two-Higgs-doublet models at the LHC and ILC, *JHEP* **1411**, 085 (2014).
- [102] G. C. Dorsch, S. J. Huber, K. Mimasu, J. M. No, Hierarchical versus degenerate 2HDM: The LHC run 1 legacy at the onset of run 2, *Phys. Rev. D* **93**, 115033 (2016).
- [103] F. Kling, J. M. No, S. Su, Anatomy of Exotic Higgs Decays in 2HDM, *JHEP* **1609**, 093 (2016).
- [104] A. Biswas, A. Lahiri, Alignment, reverse alignment, and wrong sign Yukawa couplings in two Higgs doublet models, *Phys. Rev. D* **93**, 115017 (2016).
- [105] T. Modak, J. C. Romao, S. Sadhukhan, J. P. Silva, R. Srivastava, Constraining wrong-sign $hb\bar{b}bb$ couplings with $h \rightarrow \Upsilon\gamma$, *Phys. Rev. D* **94**, 075017 (2016).
- [106] P. M. Ferreira, S. Liebler, J. Wittbrodt, $pp \rightarrow A \rightarrow Zh$ and the wrong-sign limit of the two-Higgs-doublet model, *Phys. Rev. D* **97**, 055008 (2018).

- [107] L. Wang, F. Zhang, X.-F. Han, Two-Higgs-doublet model of type-II confronted with the LHC run-I and run-II data, *Phys. Rev. D* **95**, (2017) 115014.
- [108] N. Ghosh, J. Lahiri, Generalized 2HDM with wrong-sign lepton-Yukawa coupling, in light of $g_\mu - 2$ and lepton flavor violation at the future LHC, *Eur. Phys. Jour. C* **81**, (2021) 1074.
- [109] W. Su, Probing loop effects in wrong-sign Yukawa coupling region of Type-II 2HDM, *Eur. Phys. Jour. C* **81**, (2021) 404.
- [110] N. Ghosh, J. Lahiri, Generalized 2HDM with wrong-sign lepton-Yukawa coupling, in light of $g_\mu - 2$ and lepton flavor violation at the future LHC, *Eur. Phys. Jour. C* **81**, (2021) 1074.
- [111] R. V. Harlander, S. Liebler, H. Mantler, SusHi: A program for the calculation of Higgs production in gluon fusion and bottom-quark annihilation in the Standard Model and the MSSM, *Comput. Phys. Commun.* **184**, 1605 (2013).
- [112] D. Eriksson, J. Rathsman, O. Stål, 2HDMC: Two-Higgs-Doublet Model Calculator Physics and Manual, *Comput. Phys. Commun.* **181**, (2010) 189.
- [113] X.-F. Han, L. Wang, Y. Zhang, Dark matter, electroweak phase transition, and gravitational waves in the type II two-Higgs-doublet model with a singlet scalar field, *Phys. Rev. D* **103**, (2021) 035012.
- [114] ATLAS Collaboration, Search for additional heavy neutral Higgs and gauge bosons in the ditau final state produced in 36 fb^{-1} of pp collisions at $\sqrt{s}= 13 \text{ TeV}$ with the ATLAS detector, *JHEP* **1801**, 055 (2018).
- [115] ATLAS Collaboration, Search for heavy Higgs bosons decaying into two tau leptons with the ATLAS detector using p p collisions at at $\sqrt{s}= 13 \text{ TeV}$, arXiv:2002.12223.
- [116] CMS Collaboration, Search for heavy Higgs bosons decaying to a top quark pair in proton-proton collisions at $\sqrt{s}= 13 \text{ TeV}$, *JHEP* **2004**, (2020) 171.
- [117] CMS Collaboration, Search for new resonances in the diphoton final state in the mass range between 70 and 110 GeV in pp collisions at $\sqrt{s} = 8$ and 13 TeV, CMS-PAS-HIG-17-013.
- [118] ATLAS Collaboration, Search for WW/WZ resonance production in $\ell\nu q\bar{q}$ final states in pp collisions at $\sqrt{s} = 13 \text{ TeV}$ with the ATLAS detector, arXiv:1710.07235.
- [119] ATLAS Collaboration, Search for heavy resonances decaying into WW in the $e\nu\mu\nu$ final state in pp collisions $\sqrt{s} = 13 \text{ TeV}$ with the ATLAS detector,” *Eur. Phys. Jour. C* **78**, 24 (2018).
- [120] CMS Collaboration, Search for a heavy Higgs boson decaying to a pair of W bosons in proton-proton collisions at $\sqrt{s} = 13 \text{ TeV}$, arXiv:1912.01594.
- [121] ATLAS Collaboration, Search for heavy ZZ resonances in the $\ell^+\ell^-\ell^+\ell^-$ and $\ell^+\ell^-\nu\nu$ final states using proton proton collisions at $\sqrt{s} = 13 \text{ TeV}$ with the ATLAS detector, arXiv:1712.06386.
- [122] ATLAS Collaboration, Searches for heavy ZZ and ZW resonances in the $\ell\ell q\bar{q}$ and $\nu\nu q\bar{q}$ final states in pp collisions at $\sqrt{s} = 13 \text{ TeV}$ with the ATLAS detector, arXiv:1708.09638.
- [123] ATLAS Collaboration, Search for heavy resonances decaying into a pair of Z bosons in the $\ell^+\ell^-\ell'^+\ell'^-$ and $\ell^+\ell^-\nu\bar{\nu}$ final states using 139 fb^{-1} of proton–proton collisions at $\sqrt{s} \text{ TeV}$ with the ATLAS detector, *Eur. Phys. Jour. C* **81**, (2021) 332.

- [124] CMS Collaboration, Search for a massive resonance decaying to a pair of Higgs bosons in the four b quark final state in proton-proton collisions at $\sqrt{s} = 13$ TeV, arXiv:1710.04960.
- [125] CMS Collaboration, Search for Higgs boson pair production in events with two bottom quarks and two tau leptons in proton-proton collisions at $\sqrt{s} = 13$ TeV, arXiv:1707.02909.
- [126] CMS Collaboration, Combination of searches for Higgs boson pair production in proton-proton collisions at $\sqrt{s} = 13$ TeV, Phys. Rev. Lett. **122**, 121803 (2019).
- [127] CMS Collaboration, Search for resonant pair production of Higgs bosons in the $bbZZ$ channel in proton-proton collisions at $\sqrt{s} = 13$ TeV, arXiv:2006.06391.
- [128] ATLAS Collaboration, Reconstruction and identification of boosted di- τ systems in a search for Higgs boson pairs using 13 TeV proton-proton collision data in ATLAS, arXiv:2007.14811.
- [129] ATLAS Collaboration, Search for heavy resonances decaying into a W or Z boson and a Higgs boson in final states with leptons and b-jets in $36 fb^{-1}$ of $\sqrt{s} = 13$ pp collisions with the ATLAS detector, arXiv:1712.06518.
- [130] CMS Collaboration, Search for a heavy pseudoscalar boson decaying to a Z and a Higgs boson at $\sqrt{s} = 13$ TeV, Eur. Phys. Jour. C **79**, 564 (2019).
- [131] CMS Collaboration, Search for a heavy pseudoscalar Higgs boson decaying into a 125 GeV Higgs boson and a Z boson in final states with two tau and two light leptons at $\sqrt{s} = 13$ TeV, arXiv:1910.11634.
- [132] ATLAS Collaboration, Search for a heavy Higgs boson decaying into a Z boson and another heavy Higgs boson in the $\ell\ell bb$ final state in p p collisions $\sqrt{s}=13$ TeV with the ATLAS detector, Phys. Lett. B **783**, 392 (2018).
- [133] CMS Collaboration, Search for new neutral Higgs bosons through the $H \rightarrow ZA \rightarrow \ell^+\ell^-b\bar{b}$ process in pp collisions at $\sqrt{s}=13$ TeV, arXiv:1911.03781.
- [134] N. Chen, T. Han, S. Li, S. Su, W. Su, Type-I 2HDM under the Higgs and Electroweak Precision Measurements, JHEP **08**, (2020) 131.
- [135] K. Cheung, A. Jueid, J. Kim, S. Lee, C.-T. Lu, Comprehensive study of the light charged Higgs boson in the type-I two-Higgs-doublet model, Phys. Rev. D **105**, (2022) 095044.
- [136] L. Wang, Inflation, electroweak phase transition, and Higgs searches at the LHC in the two-Higgs-doublet model, arXiv:2105.02143.
- [137] O. Atkinson, M. Black, C. Englert, A. Lenz, A. Rusov, The Flavourful Present and Future of 2HDMs at the Collider Energy Frontier, arXiv:2202.08807.
- [138] O. Atkinson, M. Black, A. Lenz, A. Rusov, J. Wynne, Cornering the Two Higgs Doublet Model Type II, JHEP **04**, (2022) 172.
- [139] F. Kling, S. Su, W. Su, 2HDM Neutral Scalars under the LHC, JHEP **06**, (2020) 163.
- [140] H. E. Haber, J. P. Silva, Exceptional regions of the 2HDM parameter space, Phys. Rev. D **103**, (2021) 115012.
- [141] S. Kanemura, M. Takeuchi, K. Yagyu, Probing double-aligned two Higgs doublet models at LHC, Phys. Rev. D **105**, (2022) 115001.

- [142] M. Aiko, S. Kanemura, M. Kikuchi, K. Mawatari, K. Sakurai, K. Yagyu, Probing extended Higgs sectors by the synergy between direct searches at the LHC and precision tests at future lepton colliders, *Nucl. Phys. B* **966**, (2021) 115375.
- [143] A. Banerjee, G. Bhattacharyya, Probing the Higgs boson through Yukawa force, *Nucl. Phys. B* **961**, (2020) 115261.
- [144] F. Arco, S. Heinemeyer, M. J. Herrero, Exploring sizable triple Higgs couplings in the 2HDM, *Eur. Phys. Jour. C* **80**, (2020) 884.
- [145] E. Lundstrom, M. Gustafsson, J. Edsjo, The Inert Doublet Model and LEP II Limits, *Phys. Rev. D* **79**, 035013 (2009).
- [146] A. Pierce, J. Thaler, Natural Dark Matter from an Unnatural Higgs Boson and New Colored Particles at the TeV Scale, *JHEP* **08**, 026 (2007).
- [147] D. Majumdar, A. Ghosal, Dark Matter candidate in a Heavy Higgs Model - Direct Detection Rates *Mod. Phys. Lett. A* **23**, (2008) 2011.
- [148] M. Gustafsson, E. Lundstrom, L. Bergstrom, J. Edsjo, Significant Gamma Lines from Inert Higgs Dark Matter, *Phys. Rev. Lett.* **99**, 041301 (2007).
- [149] M. Aoki, S. Kanemura and H. Yokoya, Reconstruction of Inert Doublet Scalars at the International Linear Collider, *Phys. Lett. B* **725**, 302 (2013).
- [150] Q.-H. Cao, E. Ma, G. Rajasekaran, Observing the dark scalar doublet and its impact on the standard-model Higgs boson at colliders, *Phys. Rev. D* **76**, 095011 (2007).
- [151] E. M. Dolle and S. Su, Inert dark matter, *Phys. Rev. D* **80**, 055012 (2009).
- [152] L. Lopez Honorez and C. E. Yaguna, The inert doublet model of dark matter revisited, *JHEP* **09**, 046 (2010).
- [153] P. Agrawal, E. M. Dolle and C. A. Krenke, Signals of inert doublet dark matter in neutrino telescopes, *Phys. Rev. D* **79**, 015015 (2009).
- [154] E. Nezri, M. H. G. Tytgat and G. Vertongen, e^+ and anti-p from inert doublet model dark matter, *JCAP* **04**, 014 (2009).
- [155] L. Lopez Honorez, C.E. Yaguna, A new viable region of the inert doublet model, *JCAP* **01**, 002 (2011).
- [156] A. Belyaev, G. Cacciapaglia, I. P. Ivanov, F. R. -Abatte, M. Thomas, Anatomy of the Inert Two Higgs Doublet Model in the light of the LHC and non-LHC Dark Matter Searches, *Phys. Rev. D* **97**, (2018) 035011.
- [157] S. Banerjee, F. Boudjema, N. Chakrabarty, H. Sun, Relic density of dark matter in the inert doublet model beyond leading order for the low mass region: 3. Annihilation in 3-body final state, *Phys. Rev. D* **104**, (2021) 075004.
- [158] A. Ilnicka, M. Krawczyk, T. Robens, Inert Doublet Model in light of LHC Run I and astrophysical data, *Phys. Rev. D* **93**, (2016) 055026.
- [159] G. Jungman, M. Kamionkowski, K. Griest, Supersymmetric dark matter, *Phys. Rept.* **267**, 195 (1996); M. A. Shifman, A. I. Vainshtein and V. I. Zakharov, Remarks on Higgs Boson Interactions with Nucleons, *Phys. Lett. B* **78**, 443 (1978).

- [160] A. Crivellin, M. Hoferichter, M. Procura, Phys. Rev. D **89**, 054021 (2014).
- [161] S. Li, Y. Xiao and J. M. Yang, A pedagogical review on muon $g - 2$, Physics 4 (2021) 40.
- [162] B. Abi *et al.* [Muon $g-2$ Collaboration], Measurement of the Positive Muon Anomalous Magnetic Moment to 0.46 ppm, Phys. Rev. Lett. **126**, (2021) 141801.
- [163] G. W. Bennett *et al.* [Muon $g-2$ Collaboration], Final report of the E821 muon anomalous magnetic moment measurement at BNL, Phys. Rev. D **73**, (2006) 072003.
- [164] T. Aoyama, M. Hayakawa, T. Kinoshita and M. Nio, Complete Tenth-Order QED Contribution to the Muon $g - 2$, Phys. Rev. Lett. **109**, (2012) 111808.
- [165] A. Czarnecki, W. J. Marciano and A. Vainshtein, Refinements in electroweak contributions to the muon anomalous magnetic moment, Phys. Rev. D **67**, (2003) 073006.
- [166] G. Eichmann, C. S. Fischer and R. Williams, Kaon-box contribution to the anomalous magnetic moment of the muon, Phys. Rev. D **101**, (2020) 054015.
- [167] M. Davier, A. Hoecker, B. Malaescu and Z. Zhang, A new evaluation of the hadronic vacuum polarisation contributions to the muon anomalous magnetic moment and to $\alpha(\mathbf{m}_Z^2)$, Eur. Phys. Jour. C **80**, (2020) 241.
- [168] M. Abdughani, K. Hikasa, L. Wu, J. M. Yang, J. Zhao, Testing electroweak SUSY for muon $g - 2$ and dark matter at the LHC and beyond, JHEP **11**, 095 (2019).
- [169] P. Athron, C. Balázs, D. H. J. Jacob, W. Kotlarski, D. Stöckinger and H. Stöckinger-Kim, New physics explanations of α_μ in light of the FNAL muon $g - 2$ measurement, JHEP **09**, 080 (2021).
- [170] F. Wang, L. Wu, Y. Xiao, J. M. Yang, Y. Zhang, GUT-scale constrained SUSY in light of new muon $g - 2$ measurement, Nucl. Phys. B **970**, 115486 (2021).
- [171] M. Endo, K. Hamaguchi, S. Iwamoto, T. Kitahara, Supersymmetric interpretation of the muon $g - 2$ anomaly, JHEP **07**, 075 (2021).
- [172] B. Lautrup, A. Peterman and E. de Rafael, The muon $g - 2$ precession experiments: past, present and future, Phys. Rept. **3**, (1972) 193.
- [173] J. P. Leveille, The second order weak correction to $g - 2$ of the muon in arbitrary gauge models, Nucl. Phys. B **137**, (1978) 63.
- [174] A. Dedes and H. E. Haber, Can the Higgs sector contribute significantly to the muon anomalous magnetic moment?, JHEP **0105**, (2001) 006.
- [175] D. Chang, W.-F. Chang, C.-H. Chou, W.-Y. Keung, Large two loop contributions to $g - 2$ from a generic pseudoscalar boson, Phys. Rev. D **63**, (2001) 091301.
- [176] K.-m. Cheung, C.-H. Chou and O.C.W. Kong, Muon anomalous magnetic moment, two Higgs doublet model and supersymmetry, Phys. Rev. D **64**, (2001) 111301.
- [177] K. Cheung, O.C.W. Kong, Can the two Higgs doublet model survive the constraint from the muon anomalous magnetic moment as suggested?, Phys. Rev. D **68**, (2003) 053003.
- [178] P. Athron, C. Balazs, A. Cherchiglia, D. H. J. Jacob, D. Stockinger, H. Stockinger-Kim, A. Voigt, Eur. Phys. Jour. C **82**, (2022) 229.

- [179] S. Schael et al. [ALEPH and DELPHI and L3 and OPAL and SLD and LEP Electroweak Working Group and SLD Electroweak Group and SLD Heavy Flavour Group Collaborations], Phys. Rept. **427**, (2006) 257.
- [180] Y. Amhis et al. [Heavy Flavor Averaging Group (HFAG) Collaboration], Averages of b-hadron, c-hadron, and τ -lepton properties as of summer 2014, arXiv:1412.7515.
- [181] D. Dercks, N. Desai, J. S. Kim, K. Rolbiecki, J. Tattersall and T. Weber, CheckMATE 2: From the model to the limit, Comput. Phys. Commun. **221**, (2017) 383.
- [182] A. M. Sirunyan *et al.* [CMS Collaboration], Combined search for electroweak production of charginos and neutralinos in proton-proton collisions at $\sqrt{s} = 13$ TeV, JHEP **1803**, (2018) 160.
- [183] A. M. Sirunyan *et al.* [CMS Collaboration], Search for electroweak production of charginos and neutralinos in multilepton final states in proton-proton collisions at $\sqrt{s} = 13$ TeV, JHEP **1803**, (2018) 166.
- [184] A. M. Sirunyan *et al.* [CMS Collaboration], Search for new phenomena in final states with two opposite-charge, same-flavor leptons, jets, and missing transverse momentum in pp collisions at $\sqrt{s} = 13$ TeV, JHEP **1803**, (2018) 076.
- [185] A. M. Sirunyan *et al.* [CMS Collaboration], Search for electroweak production of charginos and neutralinos in WH events in proton-proton collisions at $\sqrt{s} = 13$ TeV, JHEP **1711**, (2017) 029.
- [186] M. Aaboud *et al.* [ATLAS Collaboration], Search for the direct production of charginos and neutralinos in final states with tau leptons in $\sqrt{s} = 13$ TeV pp collisions with the ATLAS detector, Eur. Phys. J. C **78**, (2018) 154.
- [187] X.-F. Han, T. Li, L. Wang, Y. Zhang, Simple interpretations of lepton anomalies in the lepton-specific inert two-Higgs-doublet model, Phys. Rev. D **99**, (2019) 095034.
- [188] X.-F. Han, T. Li, H.-X. Wang, L. Wang, Y. Zhang, Lepton-specific inert two-Higgs-doublet model confronted with the new results for muon and electron $g - 2$ anomalies and multilepton searches at the LHC, Phys. Rev. D **104**, (2021) 115001.
- [189] R. H. Parker, C. Yu, W. Zhong, B. Estey, H. Mueller, Measurement of the fine-structure constant as a test of the Standard Model, Science **360**, (2018) 191.
- [190] D. Hanneke, S. Fogwell and G. Gabrielse, New Measurement of the Electron Magnetic Moment and the Fine Structure Constant, Phys. Rev. Lett. **100**, 120801 (2008).
- [191] D. Hanneke, S. F. Hoogerheide and G. Gabrielse, Cavity Control of a Single-Electron Quantum Cyclotron: Measuring the Electron Magnetic Moment, Phys. Rev. A **83**, 052122 (2011).
- [192] L. Morel, Z. Yao, P. Cladé and S. Guellati-Khélifa, Determination of the fine-structure constant with an accuracy of 81 parts per trillion, Nature **588**, (2020) 7836, 61–65.
- [193] S. Li, Y. Xiao, J. M. Yang, Can electron and muon $g - 2$ anomalies be jointly explained in SUSY?, arXiv:2107.04962.
- [194] Y. Abe, T. Toma, K. Tsumura, A μ - τ -philic scalar doublet under Z_n flavor symmetry, JHEP **1906**, (2019) 142.
- [195] S. Davidson, G. J. Grenier, Lepton flavour violating Higgs and tau to mu gamma, Phys. Rev. D **81**, (2010) 095016.

- [196] K. A. Assamagan, A. Deandrea, P.-A. Delsart, Search for the lepton flavor violating decay $A^0/H^0 \rightarrow \tau^\pm \mu^\mp$ at hadron colliders, *Phys. Rev. D* **67**, (2003) 035001.
- [197] Y. Zhou, Y.-L. Wu, Lepton flavor changing scalar interactions and muon $g-2$, *Eur. Phys. Jour. C* **27**, (2003) 577.
- [198] L. Wang, Y. Zhang, μ - τ -philic Higgs doublet model confronted with the muon $g-2$, τ decays, and LHC data, *Phys. Rev. D* **100**, (2019) 095005.
- [199] S. Iguro, Y. Omura, M. Takeuchi, Testing the 2HDM explanation of the muon $g-2$ anomaly at the LHC, *JHEP* **11**, (2019) 130.
- [200] H.-X. Wang, L. Wang, Y. Zhang, Muon $g-2$ anomaly and μ - τ -philic Higgs doublet with a light CP-even component, *Eur. Phys. Jour. C* **81**, (2021) 1007.
- [201] T. Abe, R. Sato, K. Yagyu, Muon specific two-Higgs-doublet model, *JHEP* **07**, 012 (2017).
- [202] F. J. Botella, F. Cornet-Gomez, M. Nebot, Electron and muon $g-2$ anomalies in general flavour conserving two Higgs doublets models, *Phys. Rev. D* **102**, (2020) 035023.
- [203] S. Jana, Vishnu P. K., S. Saad, Resolving electron and muon $g-2$ within the 2HDM, *Phys. Rev. D* **101**, (2020) 115037.
- [204] L.T. Hue, A. E. C. Hernandez, H. N. Long, T. T. Hong, Heavy singly charged Higgs bosons and inverse seesaw neutrinos as origins of large $(g-2)_{e,\mu}$ in two higgs doublet models, arXiv:2110.01356.
- [205] V. Ilisie, New Barr-Zee contributions to $(g-2)_\mu$ in two-Higgs-doublet models, *JHEP* **1504**, (2015) 077.
- [206] S.-P. Li, X.-Q. Li, Y. Li, Y.-D. Yang, X. Zhang, Power-aligned 2HDM: a correlative perspective on $(g-2)_{e,\mu}$, *JHEP* **2101**, (2021) 034.
- [207] O. Eberhardt, A. Martínez, A. Pich, Global fits in the Aligned Two-Higgs-Doublet model, *JHEP* **2105**, (2021) 005.
- [208] F. J. Botella, F. Cornet-Gomez, M. Nebot, Electron and muon $g-2$ anomalies in general flavour conserving two Higgs doublets models, *Phys. Rev. D* **102**, 035023 (2020).
- [209] N. Ghosh, J. Lahiri, Generalized 2HDM with wrong-sign lepton-Yukawa coupling, in light of $g_\mu-2$ and lepton flavor violation at the future LHC, *Eur. Phys. Jour. C* **81**, (2021) 1074.
- [210] L. D. Rose, S. Khalil, S. Moretti, Explaining electron and muon $g-2$ anomalies in an Aligned 2-Higgs Doublet Model with right-handed neutrinos, *Phys. Lett. B* **816**, (2021) 136216.
- [211] P. Athron, C. Balazs, T. E. Gonzalo, D. Jacob, F. Mahmoudi, Likelihood analysis of the flavour anomalies and $g-2$ in the general two Higgs doublet model, *JHEP* **01**, (2022) 037.
- [212] W. Hou, R. Jain, C. Kao, G. Kumar, T. Modak, Collider Prospects for Muon $g-2$ in General Two Higgs Doublet Model, *Phys. Rev. D* **104**, (2021) 075036.
- [213] N. Ghosh, J. Lahiri, Revisiting a generalized two-Higgs-doublet model in light of the muon anomaly and lepton flavor violating decays at the HL-LHC, *Phys. Rev. D* **103**, (2021) 055009.
- [214] S. Iguro, Y. Omura, M. Takeuchi, Probing $\mu\tau$ flavor-violating solutions for the muon $g-2$ anomaly at Belle II, *JHEP* **09**, (2020) 144.

- [215] T. Li, M. A. Schmidt, C.-Y. Yao, M. Yuan, Charged lepton flavor violation in light of the muon magnetic moment anomaly and colliders, *Eur. Phys. Jour. C* **81**, (2021) 811.
- [216] M. Lindner, M. Platscher, F. S. Queiroz, A Call for New Physics : The Muon Anomalous Magnetic Moment and Lepton Flavor Violation, *Phys. Rept.* **731**, (2018) 1-82.
- [217] P. S. B. Dev, R. N. Mohapatra, Y. Zhang, Lepton Flavor Violation Induced by a Neutral Scalar at Future Lepton Colliders, *Phys. Rev. Lett.* **120**, 221804 (2018).
- [218] F. Wang, W. Wang, J. M. Yang, Y. Zhang, B. Zhu, Low energy supersymmetry confronted with current experiments: an overview, *arXiv:2201.00156*.
- [219] H. Baer, V. Barger, S. Salam, D. Sengupta, K. Sinha, Status of weak scale supersymmetry after LHC Run 2 and ton-scale noble liquid WIMP searches, *Eur. Phys. J. ST* **229**, 3085 (2020).